U. S. AIR FORCE

PROJECT RAND

RESEARCH MEMORANDUM

A CALCULATION OF THE BLAST WAVE FROM A SPHERICAL CHARGE OF TNT

Harold L. Brode

RM-1965

ASTIA Document Number AD 144302

21 August 1957

Assigned to _____

The RAND Corporation
1700 MAIN ST. • SANTA MONICA • CALIFORNIA

CONTENTS

ABSTRACT v

I. INTRODUCTION 1

II. EQUATIONS OF MOTION 3

III. EQUATIONS OF STATE 7

Equation of State of TNT 9

IV. INITIAL CONDITIONS AND SCALING 15

V. RESULTS 17

REFERENCES 24

ABSTRACT

The numerical solution of the partial differential equations of hydrodynamic motion for the case of a center-detonated spherical charge of TNT was accomplished on a high speed computer. Detailed equations of state for air and TNT were used. Results are shown principally in graphical form, in which the second shock is seen to originate as an imploding shock following the inward rarefaction into the TNT gases. A series of minor shocks are generated in the same manner and are seen to move out in the negative phase behind the main shock.

I. INTRODUCTION

In the considerable study devoted to high explosive detonations and their resulting blast waves much use has been made of experimental information. (The first three references are examples of the exhaustive analyses possible from such data.) With the more powerful computational aids now available it is possible to develop solutions to detonation problems without reliance on empirical values derived from explosion measurements. One such solution is reported on here. The hydrodynamical equations of motion, which constitute a set of nonlinear partial differential equations, were integrated by a numerical procedure on a high speed electronic computer. A common form of the artificial viscosity technique of von Neumann and Richtmyer[4] was used here, as in earlier work.[5] The initial conditions for this particular blast calculation were approximately those of the centered detonation of a bare sphere to TNT of loading density 1.5 g/cm^3 as specified by the detonation wave descriptions of Taylor.[6] The equation of state of this TNT was modeled after that of Jones and Miller,[7] while the equation of state of air was a fit to computed data of several authors but primarily that of Gilmore[8] and of Hilsenrath and Beckett.[9]

The results show clearly the details of the main shock in air, the rarefaction into the high explosive gases, the second shock (one which follows the rarefaction wave), and various subsequent reflections and refractions of the second shock between the origin and the contact surface. Comparison with the results of a mass-less point-source explosion illustrates the lasting effects on the blast wave of the initial mass and energy distribution in a high explosive detonation.

II. EQUATIONS OF MOTION

The equations of motion may be expressed in a Lagrangean form with the independent variables being the time (t) and a mass coordinate (X) where X is defined as $X = \rho_1 r_o^3/3$ (i.e., the mass per steradian) for which ρ_1 is the initial density of the gas and r_o its initial radius. The hydrodynamic equations for spherical symmetry may then be written as follows:

$$\frac{1}{\rho} = R^2 \frac{\partial R}{\partial X}, \qquad \text{conservation of mass;} \qquad (1)$$

$$\frac{\partial u}{\partial t} = - R^2 \frac{\partial P}{\partial X}, \qquad \text{conservation of momentum;} \qquad (2)$$

$$\frac{\partial E}{\partial t} = \frac{P}{\rho^2} \frac{\partial \rho}{\partial t}, \qquad \text{conservation of energy;} \qquad (3)$$

$$P(E,\rho), \qquad \text{caloric equation of state;} \qquad (4)$$

$$T(E,\rho), \qquad \text{thermal equation of state;} \qquad (5)$$

$$u = \frac{\partial R}{\partial t}, \qquad \text{definition of particle velocity} \qquad (6)$$

in which ρ is the density, R is the radial position, u is the particle velocity, P is the pressure, E is the internal energy and T is the temperature.

It is convenient to reduce these equations to a dimensionless set which then may be applied to any initial total energy (w) and any initial pre-shock conditions (P_o, ρ_o, T_o, E_o), where these ambient units are related as follows:

$$a^3 = \frac{w}{P_o}, \tag{7}$$

$$E_o = \frac{P_o}{\rho_o(\gamma_o - 1)} \text{ or } \frac{P_o}{\rho_o E_o} = (\gamma_o - 1) = 0.4, \tag{8}$$

$$C_o^2 = \frac{\gamma_o P_o}{\rho_o} \text{ or } \frac{C_o^2 \rho_o}{P_o} = \gamma_o = 1.4. \tag{9}$$

Defining the following reduced variables,

$$\begin{aligned}
&\pi = P/P_o && \text{(pressure in atmos)} \\
&\eta = \rho/\rho_o && \text{(density relative to ambient air)} \\
&\beta = u/C_o && \text{(mass or particle speed-Mach No.)} \\
&\varepsilon = E/E_o && \text{(internal energy relative to ambient air)} \\
&\theta = T/T_o && \text{(temperature relative to standard temp., } {}^oK) \\
&\lambda = R/a && \text{(reduced radius)} \\
&x = X/\rho_o a^3 = \frac{\eta_1 \lambda_o^3}{3} = \frac{1}{3}\frac{\rho_1 r_o^3}{\rho_o a^3} && \text{(mass units)} \\
&\lambda_o = r_o/a \\
&\tau = tC_o/a && \text{(reduced time)}
\end{aligned} \tag{10}$$

the equations of motion become

$$\frac{1}{\eta} = \lambda^2 \frac{\partial \lambda}{\partial x} = \frac{1}{3} \frac{\partial \lambda^3}{\partial x} \tag{11}$$

$$\frac{\partial \beta}{\partial \tau} = - \frac{1}{\gamma_o} \lambda^2 \frac{\partial \pi}{\partial x} \tag{12}$$

$$\frac{\partial \epsilon}{\partial \tau} = (\gamma_o - 1) \frac{\pi}{\eta^2} \frac{\partial \eta}{\partial \tau} \tag{13}$$

$$\frac{\partial \lambda}{\partial \tau} = \beta \tag{14}$$

It will be convenient to write the equations of state in still another form.

$$\theta = z\, S(z,\eta), \qquad \text{where } z = \pi/\eta, \tag{15}$$

and

$$\epsilon = (\gamma_o - 1)\,(z\,)\,(\tfrac{\mu-1}{2}); \quad \mu(z,\xi), \quad \xi = \ln \eta. \tag{16}$$

Using this expression (Eq. (16)) for ϵ in Eq. (13) leads to another form of the energy equation:

$$\frac{\partial z}{\partial \tau} = \frac{(2 - \frac{\partial \mu}{\partial \xi})z}{(\mu - 1 + z \frac{\partial \mu}{\partial z})} \frac{\partial \xi}{\partial \tau} . \tag{17}$$

In order to numerically integrate these equations from some set of initial conditions, these equations must be replaced by an appropriate set of difference equations. Details of the difference equations and of the numerical procedure followed in solving them are available elsewhere[10] and so will not be repeated here.

III. EQUATIONS OF STATE

The two functions $S(z,\eta)$ and $\mu(z,\xi)$ which are ordinarily determined by equation of state data are not entirely independent. A reciprocity relation exists which places a constraint on these functions in order that they satisfy the second law of thermodynamics. For purely hydrodynamical considerations, however, there is no need to observe this restraint since the thermal equation is superfluous to the equation of motion. In such cases where the temperature is coupled to the hydrodynamics, e.g., as by radiation, heat conduction, or heat diffusion, it should be necessary to observe the reciprocity restriction. The analytic forms introduced are intended to make such a constraint less difficult to comply with in fitting the two equations of state.

Choosing as our independent variables $z = \pi/\eta$, and ξ the second law in the form

$$ds = \frac{Dq}{T} = \frac{dE + pdv}{T} \text{ , where } v = \frac{1}{\rho} \text{ ,} \tag{18}$$

becomes

$$\frac{\rho_o T_o}{P_o} ds = \frac{1}{2S(z,\xi)} \left\{ \left(\frac{\partial \mu}{\partial \xi}\right)_z d\xi + \left[\left(\frac{\partial \mu}{\partial z}\right)_\xi + \frac{\mu - 1}{z} \right] dz \right\} - \frac{d\xi}{\xi} \tag{19}$$

$$= \left[\frac{1}{2S} \left(\frac{\partial \mu}{\partial \xi}\right)_z - \frac{1}{S} \right] d\xi + \frac{1}{2S} \left[\left(\frac{\partial \mu}{\partial z}\right)_\xi + \frac{\mu - 1}{z} \right] dz,$$

and in order that ds be a perfect differential, the following reciprocity relation must hold:

$$\frac{\partial}{\partial z}\left[\frac{1}{2S}\left(\frac{\partial \mu}{\partial \xi}\right)_z - \frac{1}{S}\right] = \frac{\partial}{\partial \xi}\left[\frac{1}{2S}\left(\frac{\partial \mu}{\partial z}\right)_\xi + \frac{\mu-1}{2zS}\right] . \tag{20}$$

To within 10 per cent in the density range of interest the function S can represent the thermal properties of air as a function of z alone (independent of ξ). Furthermore, the function μ can fit the caloric properties to the same accuracy with the form

$$\mu = \mu_o(z) + \mu_1(z)\xi \quad . \tag{21}$$

In this case, then, the reciprocity relation requires that

$$\mu_1(z) = \frac{2zS'}{S+zS'} . \tag{22}$$

The equation of state of air data were taken from Refs. 11, 12 and 13 and were subsequently revised to the later information of Refs. 8 and 9. The fits used are as follows:

$$\frac{T}{T_o} = \theta = z\, S(z)$$

$$S(z) = \frac{485}{1000 + z^2} + \frac{3860\, z}{7500 + 16.5\, z} \tag{23}$$

$$\frac{E}{E_o} = \varepsilon = \frac{(\gamma_o - 1)}{2}\, z\, (\mu-1)$$

$$\mu = \mu_o + 0.09\,(\mu_o - \mu_2)\,\xi \tag{24}$$

$$\mu_2 = \frac{6002\, y + 4}{1000\, y + 1}$$

where $y = z^{-1}$

$$\mu_o = 1 + \frac{25.89486848y + 3}{4.778973696y + 1} + \frac{861(1-y)y}{3000y^2 + 1} + \frac{2356(1-y)y}{9 \times 10^4 y^2 + 1} + \frac{41,000(1-y)y}{12 \times 10^6 y^2 + 1}.$$

Equation of State of TNT

It is necessary that the detonation products have an internal energy plus kinetic energy equal to the net energy release by chemical reaction. Jones and Miller[7] indicate a net energy release of 247.9 K Cal/mole of TNT (at 1.5 gm/cc loading density) after the gas products have expanded to more than three times their initial volume and the temperature has dropped below 1600°K (for this loading density).

At the detonation front the chemical energy release is 288.6 K Cal/mole of TNT. Part of this energy goes into the forming of such gases as carbon monoxide which increases rapidly behind the front.

The molar volume at the detonation front is given as 117 cm^3 while the density is 2 gm/cm^3, so that the molecular weight is 234 gms.

The internal energy is given approximately by Jones and Miller as

$$E = 0.0875T - 38.0 + N'E_1 \text{ Kcal/mole....,} \qquad (25)$$

where T is in degrees Kelvin, and N' is the number of moles of gas per mole of TNT, a number that goes from 5.8 at the detonation front to 7.0 when the composition becomes fixed.

E_1 is given as

$$E_1 = -1/2\ cp^2 - \frac{2}{3}\ dp^3 \text{ 1000 kg cm/mole....,} \qquad (26)$$

where $c = -0.104$, $d = 2.33 \times 10^{-4}$ and p is in 1000 kg/cm^2. By writing E_1 in Kcal/mole TNT and p in atmospheres ($p/p_o = \pi$), E_1 becomes

$$E_1 = (.0234)\left[5.564 \times 10^{-8}\pi^2 - 1.72 \times 10^{-13}\pi^3\right] \text{ Kcal/mole.... .} \quad (27)$$

Then E is

$$E = 0.0875T - 38.0 + N'(0.0234)(5.564 \times 10^{-8}\pi^2 - 1.72 \times 10^{-13}\pi^3) \text{ Kcal/mole.} \quad (28)$$

At the detonation front where $T = 3400^\circ K$, $\pi = 15.665 \times 10^4$ atmos, and $N' = 5.8$ the energy equals 355.07 Kcal/mole TNT according to this expression. Even without the $N'E_1$ term it gives 259.5 Kcal/mole TNT in contrast to the stated 288.6 Kcal/mole TNT. Furthermore this form gives negative energies below $430^\circ K$.

For the sake of a hydrodynamic calculation it is important to have the correct total energy. It is also desirable, but less important for later stages, to have it distributed approximately correctly initially. It would be convenient to have the internal energy compatible with the ideal gas behavior of the mixture near standard atmosphere conditions. This latter consideration is satisfied by an energy that near standard conditions approaches the ideal gas expression

$$E = \frac{p}{\rho(\gamma-1)}, \quad (29)$$

where γ is the same as the adiabatic γ which in this case is $\gamma = 1.27$. This is approximately satisfied by allowing E to go to $1.5E_o = 2.94 \times 10^9$ erg/gm at standard conditions.

One can assure the correctness of the total energy by adding up the internal and kinetic energies in the hydrodynamic field at a time when the composition has become fixed.

If one were to start a blast calculation from a detonation wave at the instant the detonation wave reaches the surface of a spherical charge of TNT, then he would find that none of the resulting gas has reached a fixed composition. In that case the total energy in the field should lie somewhere between the chemical energy available at the detonation front and the net chemical energy released when composition becomes fixed, i.e., between 288.6 Kcal/mole TNT and 247.9 Kcal/mole TNT.

Using the equation of state as given (Eq. 28) and the conditions behind the detonation front as specified by Sir Taylor[6] (Table 2, Ref. 6) and averaging over the mass distribution of the spherical charge, the total energy per mole of TNT can be computed.

$$E_{tot} = E_{kinetic} + E_{internal} = E_k + E_i \tag{30}$$

$$E_i = 4\pi R^3 \int_0^1 E\rho y^2 dy \Big/ 4\pi R^3 \int_0^1 \rho y^2 dy = 209.8 \text{ Kcal/mole} \tag{31}$$

where $y = r/R$

$$E_k = \int_0^1 \frac{1}{2} \rho u^2 y^2 dy \Big/ \int_0^1 \rho y^2 dy = 11.90 \text{ Kcal/mole} \tag{32}$$

$$E_{tot} = 221.7 \text{ Kcal/mole.} \tag{33}$$

This latter total energy is less than the net energy released and so would seem to be incorrect, or at least undesirable.

By arbitrarily increasing the additive term in E, so that E becomes

$$E = 0.0875T - 7.46 + N'E_1 \qquad \text{Kcal/mole TNT,} \qquad (34)$$

the figure for E_{tot} would become 252.28 Kcal/mole TNT and at the same time the energy at standard temperature (273.2°K) becomes 16.44 Kcal/mole TNT which is $1.5E_o$, as desired. On the other hand, this will raise the energy released at the detonation front by a corresponding amount, where we have already seen this figure to be too high by the previous form for E (Eq. (28)). Since an incorrect total energy would seem to have more lasting effect than an incorrect initial distribution, we were inclined to accept this arbitrary alteration and compute accordingly.

The excessively high energies near the detonation front could be reduced by lowering the pressure or raising the density there, and correspondingly but to a lesser extent at points behind the front. Such empirical adjustments of parameters are distasteful at best and need always be done with care so that energies and densities remain in their proper proportions. This particular equation of state is itself an empirical relation intended only to approximate the effects of close packing on the gas molecules through the higher order pressure terms (where no temperature dependence has been assigned to the coefficients of these pressure terms). Consequently, we have elected to leave the pressures and densities, as described by Sir Taylor[6], unchanged, and to alter the internal energy by the constant factor (as in Eq. (34)). This results in approximately the correct average energy per mole of TNT in the detonation wave and leads to a simple form for conditions near standard air density and temperature. It does, however, lead to a

spurious signal of little consequence in the early portion of the explosion.

Using the equation of state from Jones and Miller as modified in Eq. (34), and dividing by the internal energy of air at standard conditions, (E_o = 1.96 x 10^9 erg/gm) the internal energy is

$$\varepsilon = \frac{1}{5}\left(a\theta - b + c\pi^2 N' - d\pi^3 N'\right)$$
$$= \frac{1}{5}\left(azS(z) - b + cz^2\eta^2 N' - dz^3\eta^3 N'\right). \qquad (35)$$

Also, by definition, μ and ε are related as

$$\mu = \frac{\gamma+1}{\gamma-1} = 1 + \frac{5\varepsilon}{z} = 1 + aS - \frac{b}{z} + cz\eta^2 N' - dz^2\eta^3 N' \qquad (36)$$

$$z\mu_z = aS'z + \frac{b}{z} + c\eta^2 N'z - 2dz^2\eta^3 N'. \qquad (37)$$

These expressions are a little cumbersome, so since the form of μ along the particular adiabat followed by much of the H.E. is very simply fit by the analytical form

$$\mu_{HE} \simeq a + \frac{bz}{c+z^2} + 1, \qquad (38)$$

$$a = 1.176,$$

$$b = 52.4892,$$

$$c = 7.300,$$

this simpler form was incorporated in the calculations with the understanding that it is valid only for a particular loading density of TNT (ρ_{HE} = 1.5 gm/cc).

The former, more general form should be applicable for a variety of densities. However, Jones and Miller do not state that their approximate form for the internal energy is valid for explosives other than TNT.

The approximate temperature (θ) in units of standard air temperature (T_o = 273.2°K), may be computed for the TNT gases by the form

$$\theta = zS(z), \quad S = 12/(9.65 + z), \tag{39}$$

in the range of z between detonation conditions and ambient.

IV. INITIAL CONDITIONS AND SCALING

The conditions in the detonation wave at the instant that the front reaches the surface of the bare spherical charge of TNT were taken to be those prescribed by Taylor as shown in Ref. 6, Table 2. The conditions in the air surrounding the charge were taken as standard sea level air conditions:

$$P_o = 1.01375 \times 10^6 \text{ dynes/cm}^2$$
$$\rho_o = 1.293 \times 10^{-3} \text{ grams/cm}^3$$
$$c_o = 33{,}136 \text{ cm/sec}$$
$$T_o = 273.2 \ ^oK$$

The units of the problem permit easy scaling to other atmospheres and to any energy or charge size, but since the initial conditions for the high explosive are expressed in the same units, any one solution can only be scaled to other atmospheric conditions with an accompanying and proportional change in the explosive and detonation wave conditions. This is an unavoidable limitation since in any chemical explosive detonation the blast wave will be influenced by the initial mass out to very low pressure levels--until such shock radii as would engulf a mass of air roughly ten times the mass of the explosive. For a sphere of TNT at sea level this would mean roughly 23 charge radii, or out to an overpressure of five atmospheres or about 70 psi. As will be seen in the next section (Fig. 1) this distance is about the distance where the overpressure decay rate becomes that of the point source blast wave. In the thinner atmosphere

at 40,000 feet altitude—for example, the corresponding distance where the shock has engulfed a mass of air ten times that of the explosive is more like 36 charge radii, and the overpressure there is a maximum of 17 psi. As a result of this mass effect, only at distances greater than the radius at which a mass of air of ten times the initial mass has been engulfed, is it reasonable to scale these results by the usual (Sach's) scaling. At points nearer to the explosion the effect of the initial mass should prevent simple scaling.

When the explosive loading density is scaled by the same factor as the ambient air density the results of this calculation should again be applicable. As at 40,000 feet, the scaled results should be appropriate to a TNT sphere of loading density of .375 g/cm^3 if such an explosive could exist.

V. RESULTS

The peak overpressure as a function of shock radius is shown in Fig. 1. It is interesting to note the comparison with the theoretical point-source results for air[10] and for an ideal gas of $\gamma = 1.4$.[5] Although at no stage are the TNT and point-source in air results the same, their slopes at large distances ($\lambda > 1$) become similar. The ideal gas, point-source curve shows higher pressures at the same distances, since the various dissociations and ionizations of molecules and atoms in high temperature air near the source tend to reduce the blast efficiency in real air. Since the TNT source does not shock air to extreme temperatures ($T \lesssim 9000^{\circ}K$) its later profiles indicate a greater blast efficiency than the point-source in air.

Granström has prepared a peak overpressure-distance curve for TNT of loading density 1.52 g/cm^3 which he estimates to be valid to within 5 per cent, and which he states is in agreement with the most reliable observations.[3] His curve (Fig. 25 of Ref. 3) lies beyond the curve for TNT in Fig. 1 by about 5 per cent in radius out to a λ of about 1.0, beyond which it deviates slightly more. This is a rather modest discrepancy but it nevertheless means an average blast energy efficiency of some 16 or 17 per cent greater for the Granström curve.

The deviation in the last portion of the pressure curve ($\lambda > 1.0$) is attributable to inexact treatments in the numerical procedure used for doubling and adding zones during the late stages of the calculation.

Figure 2 is a plot of the peak mass velocity or the particle Mach number ($\beta_s = \mu_s/C_o$) at the shock and the shock over-velocity or shock Mach number in excess of Mach one $\left[B-1 = (U-C_o)/C_o \right]$ versus shock radius for the main shock. Figure 3 is a similar plot of the shock compression $(\frac{\rho_s}{\rho_o} - 1)$ and the shock temperature $(\frac{T_s}{T_o} - 1)$ versus shock radius.

The positions of the main and subsequent shocks as well as the contact surface as functions of time are indicated in Fig. 4. The second shock follows a rarefaction wave into the TNT gases. It starts with zero strength and grows as it moves inward thru these gases. It is swept outward in space until the expansion of the high explosive products is nearly exhausted, then it implodes on the origin and is reflected outward to the contact surface. At the time it strikes the contact surface between the TNT gases and the air, the TNT gases are still more dense and much cooler than the air immediately outside, (this is generally true at any time). As a consequence, the shock in passing through the surface sets up an inward rarefaction wave. This rarefaction, like the initial rarefaction, is followed by a third shock moving inward. This shock, like the second implodes on the origin, reflects and moves out in the wake of the previous shocks. The succession of shocks continues in this fashion until the energy in the explosion product gases is dissipated.

The origin of these inward facing shocks lies in the necessity for a compression wave at the juncture between a spherical rarefaction wave moving away from a spherical shock wave.* No such condition exists in a plane

---

* Several "spherical shock" tube type experiments have been conducted by a group under I. I. Glass at the University of Toronto Institute of Aerophysics, and this author has provided some corresponding numerical solutions—all of which exhibit inward shocks. (Ref. 14)

shock tube--but quite in general (not just in detonations) a spherical shock wave from a source of finite volume is backed up to a rarefaction wave moving inward, and the negative pressure gradient of the rarefaction joins the positive gradient of the shock through a compression which grows as a shock as the rarefaction develops. In other terms, the shocked air, which is left at a higher entropy than the air or gases in the initial high pressure region, must be joined to these lower entropy gases at the tail of the rarefaction--and it can do so only by sending a shock into it. As the difference in the state of these adjacent gases increases with the growth of the rarefaction, the joining shock grows proportionately.

These subsidiary shocks follow the main shock at such a time and distance that they are behind the minimum of the negative phase and do not converge on or join the main shock. For a hotter gas explosion where these shocks would move out earlier--it is possible for them to overtake and join the main shock and so disappear.

The energy in the detonation wave is distributed as ninety-five per cent in internal energy or potential (pv) energy and five per cent in kinetic energy of directed motion. As the rarefaction into the dense HE gases developes, the dynamic motion or kinetic energy increases, reaching a maximum of better than sixty per cent before dissipation in the shock heating reduces it again to a low value. This changing division of energy between kinetic and internal is illustrated in Fig. 5, which shows the partition of energy as a function of time.

Figures 6 through 15 show the history of the particle velocities as a function of radius. The time is considered to be zero at the instant that the detonation wave reaches the surface of the TNT sphere. The velocities

in the detonation wave (time zero) and at a few times immediately after time zero are shown in Fig. 6. Early evidence of the second shock appears just inside the contact surface as a small jump in velocity. This second shock can be seen to grow in magnitude and to recede inward from the contact surface (see Figs. 6 through 9). At approximately $\tau = 0.136$ the second shock reaches the origin and is reflected, so that in Fig. 10 it is shown moving outward. In the first two figures, Figs. 6 and 7, there is a disturbance moving in toward the origin ahead of the rarefaction wave. This disturbance is evidently a result of the inexact match between initial conditions assumed for the detonation wave and the equation of state assumed for TNT. It does not seriously affect the results except as seen in these early curves.

A rather complicated series of shock reflections and refractions can be traced out in Fig. 11, resulting in the generation of a third and fourth shock. The earliest curve in Fig. 11 shows the second shock just after having breached the contact surface. The next curve shows a third shock moving inward, and the subsequent curves picture this third shock moving out behind the second and first shocks, generating a fourth shock in the process.

In the subsequent figures (Figs. 12 through 15) these first four shocks can be seen to continue expanding. Because of the difficulty in distinguishing further shocks, no attempt was made to indicate any more than these first four shocks.

Pressures as a function of radius at selected times are shown in Figs. 16 through 21. In the first of these, Fig. 16, the first shock can be seen to start at about 400 atmos--far below the 200,000 atmos of the detonation wave. Immediately behind the contact surface the second shock appears and grows in strength as it is forced outward by the expansion. After the rarefaction has reduced the high interior pressures to less than one tenth of an atmosphere this second shock begins to move in on the origin. Until this shock reaches the origin the pressure inside continues to drop because of the continuing rarefaction, reaching something less than 0.08 atmos before being hit by the second shock. Figure 19 shows pressure profiles before and after the implosion of this inward shock.

Figure 20 shows more of the complications due to the creation of repeated little shocks. Again no attempt is made to indicate shocks after the fourth one, although there is reason to believe that such subsidiary shocks continue to form in a similar manner.

The history of the density profiles is told by Figs. 22 through 28. The initial density of the high explosive is slightly altered by the passage of the detonation wave, but having an initial density in this problem of 1.5 g/cc, the TNT density at the start of the calculation is more than a thousand times the standard density of air. As the TNT gases expand their density is rapidly decreased. As an air shock builds up outside the surface of the TNT gases, the second shock begins to grow and move inward behind the contact surface (see Fig. 22). This results in a density profile at these times which is characterized (as one moves inward from the shock front) by first a decrease in density in the air due to the spherical expansion, second by the density discontinuity at the contact surface which

is shown by the sudden jump to higher density in the high explosive products, thirdly by the inward facing second shock which, although moving in through the mass of TNT gases, is being swept out by the general rarefaction.

In the later figures (Figs. 27 and 28) insets show the lower densities left near the origin. This low density region would eventually return to more nearly normal air density by other processes than hydrodynamics, since this represents a heated region left at a depressed density after essentially all the pv work has been done. This low density core is typical of any explosion which generates a strong shock--since the shock then raises the air and gases to a higher entropy at higher shock pressures in such a way that more heat is deposited than can be expended in subsequent expansion behind the shock.

Figure 29 shows some of the early temperature profiles where again the existence of the contact surface and the second shock somewhat complicate the picture. It should be noted that temperatures exceed two thousand degrees Kelvin for a time, rising as high as eight or nine thousand degrees in the air at the earliest times. Some radiation should be visible from this hot air during this time, but not enough energy can be lost by radiative processes to affect the hydrodynamics. The TNT gases do not exceed three thousand degrees in the detonation process and rapidly cool below that temperature in the expansion phase, but unlike the air, these gases may radiate effectively below two thousand degrees, and so may give off more light.

Figures 30 through 35 show pressures as functions of the time at selected radii. Figure 30 is a log-log plot of the pressure (in atmospheres) versus the time, showing the complicated time behavior of pressures at

distances close enough to be engulfed by the explosion products gases. Such points are at radii out to as much as ten times the charge radius. At these distances the second shock first backs through the point, then comes back in past that point, and after imploding finally comes out again. The third and fourth shocks can also be seen going in and coming out again, since by then these radii all lie inside the contact surface. Figures 31 through 35 show a more conventional overpressure-time history in which the main shock is followed by a negative overpressure phase on the back of which the second, third and subsequent shocks appear.

The durations of positive phases of overpressure and velocity are shown in Fig. 36.

Figure 37 shows the positive impulses for the overpressure and for the dynamic pressure as functions of the radius. These impulses are defined as follows:

$$I_p^+ = \int_{\tau_s}^{\tau_s + D_p^+} \Delta p \, dt, \text{ and } I_u^+ = \int_{\tau_s}^{\tau_s + D_u^+} \frac{\gamma \eta \beta^2}{2} \, dt.$$

It is interesting to note that the overpressure impulse has a dip at a point that corresponds roughly to the shock position at the time when the internal energy is a minimum and the kinetic energy is a maximum. Furthermore, the region of the dip in the overpressure impluse is one which is engulfed both by the TNT explosion product gases and by the second shock while it is being dragged backwards by the rarefaction. In a sense, the dip is artificial, due to the influence of the second shock which in this region serves as a premature end to the positive phase.

REFERENCES

1. Stoner, R. G., and W. Bleakney, "The Attenuation of Spherical Shock-Waves in Air", J. Appl. Phys., 19, (1948) p. 670-678.

2. Shardin, H., "Measurement of Spherical Shock-Waves", Commun. Pure and Appl. Math., New York University, Vol. VII, (1954) p. 223-243.

3. Granström, Sune A., Loading Characteristics of Air Blasts from Detonating Charges, Transactions of the Roy. Inst. of Tech., Stockholm) 100, (1956) (93 pages).

4. von Neumann, J., and R. D. Richtmyer, J. Appl. Phys., 21, (1950), p. 232.

5. Brode, H. L., "Numerical Solutions of Spherical Blast Waves", J. Appl. Phys., 26, (1955), p. 766.

6. Taylor, Sir Geoffrey, "The Dynamics of the Combustion Products Behind Plane and Spherical Detonation Fronts in Explosives", Proc. Roy. Soc., 200, (1950) p. 235-247.

7. Jones, H., and A. R. Miller, "The Detonation of Solid Explosives: The Equilibrium Conditions in the Detonation Wave-Front and the Adiabatic Expansion of the Products of Detonation", Proc. Roy. Soc., 194, (1948), p. 480-507.

8. Gilmore, F. R., Equilibrium Composition and Thermodynamic Properties of Air to 24,000°K, The RAND Corporation, Research Memorandum, RM-1543, August 24, 1955.

9. Hilsenrath, J., and C. W. Beckett, Thermodynamic Properties of Argon-Free Air,Nat. Bur. of Stds., Report No. 3991, April 1955.

10. Brode, H. L., Point Source Explosion in Air, The RAND Corporation, Research Memorandum, RM-1824, December 3, 1956.

11. Hirschfelder, J. O. and J. L. Magee, Thermodynamic Properties of Air at High Temperatures, Los Alamos Laboratory, LADC-122 (MDDC-590), January 1947.

12. Hirschfelder, J. O. and C. F. Curtiss, Thermodynamic Properties of Air I and II, University of Wisconsin, Reports CM-472 and CM-518, June and December 1948.

13. Krieger, F. J. and W. B. White, The Composition and Thermodynamic Properties of Air at Temperatures from 500 to 8000°K and Pressures from 0.00001 to 100 Atmos, The RAND Corporation, Report R-149, April 1949, (out of print).

14. Brode, H. L., Theoretical Solutions of Spherical Shock Tube Blasts, The RAND Corporation, Research Memorandum, RM-1974, September 4, 1957.

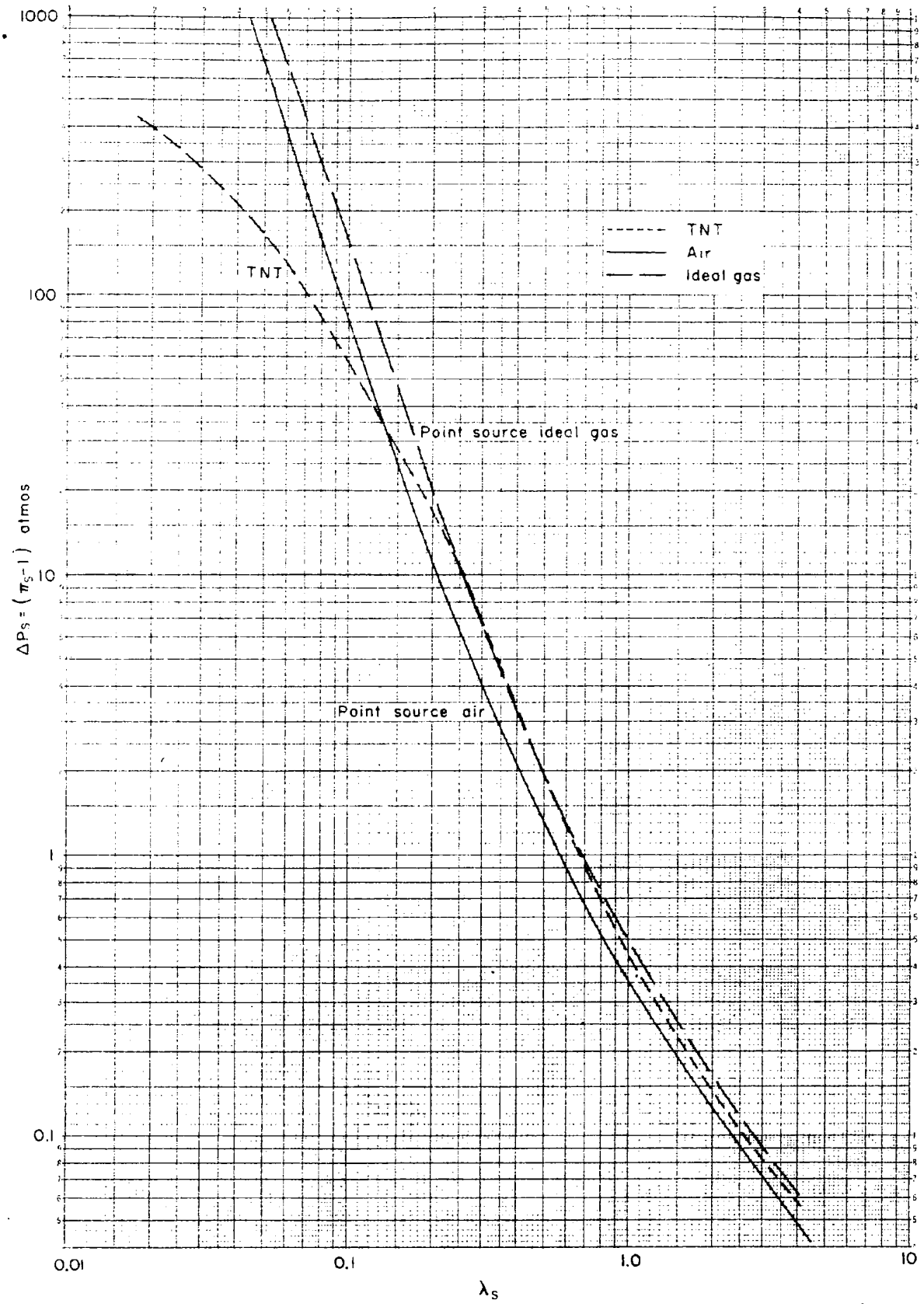

Fig.1—Peak overpressure vs shock radius $(\lambda_S = R_S/a), (a^3 = W_{TOT}/P_O)$

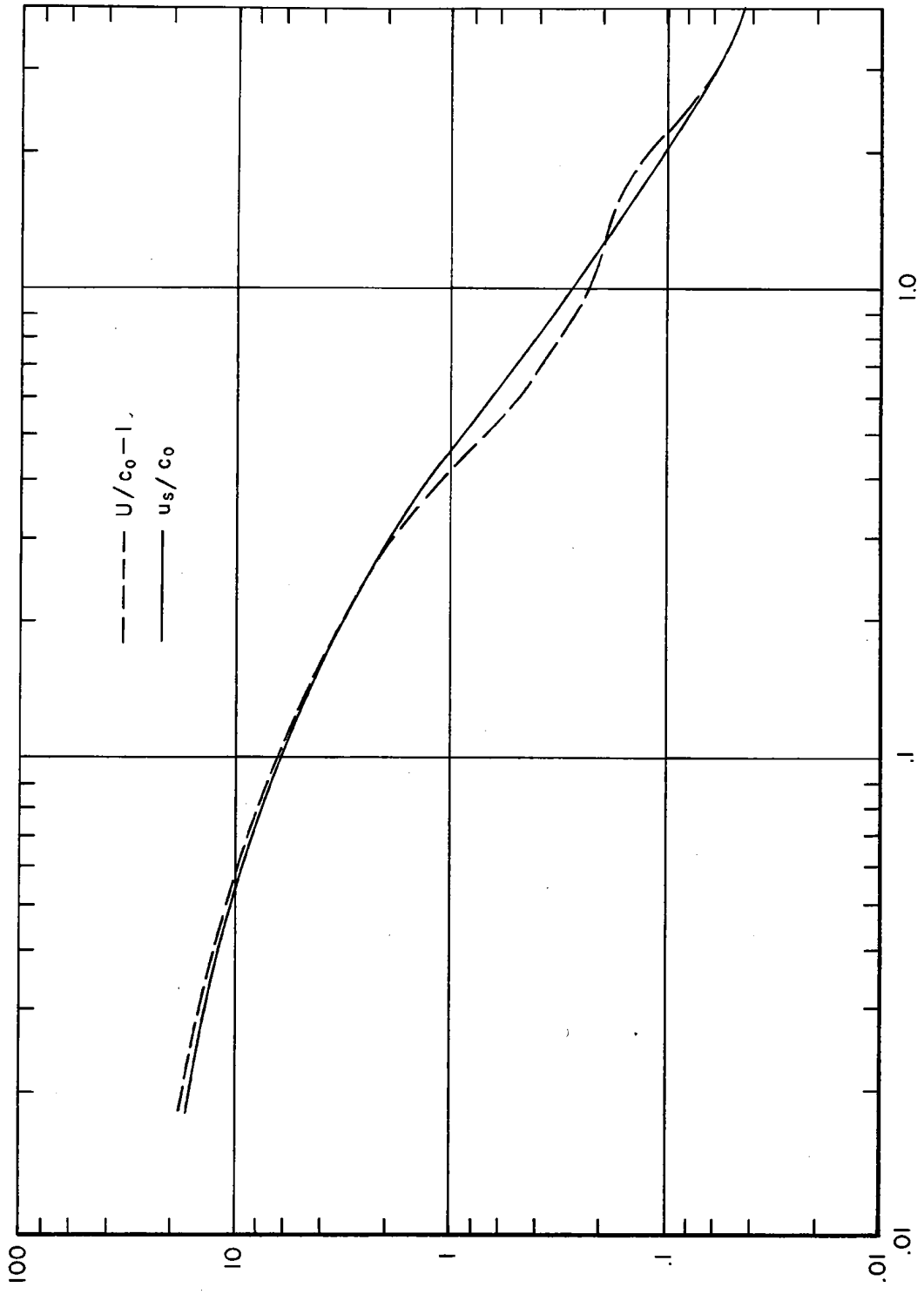

Fig. 2—Shock particle Mach number (u_S/c_O) and shock speed in excess of sound speed ($U/c_O - 1$) vs radius ($\lambda_S = R_S/a$) for TNT

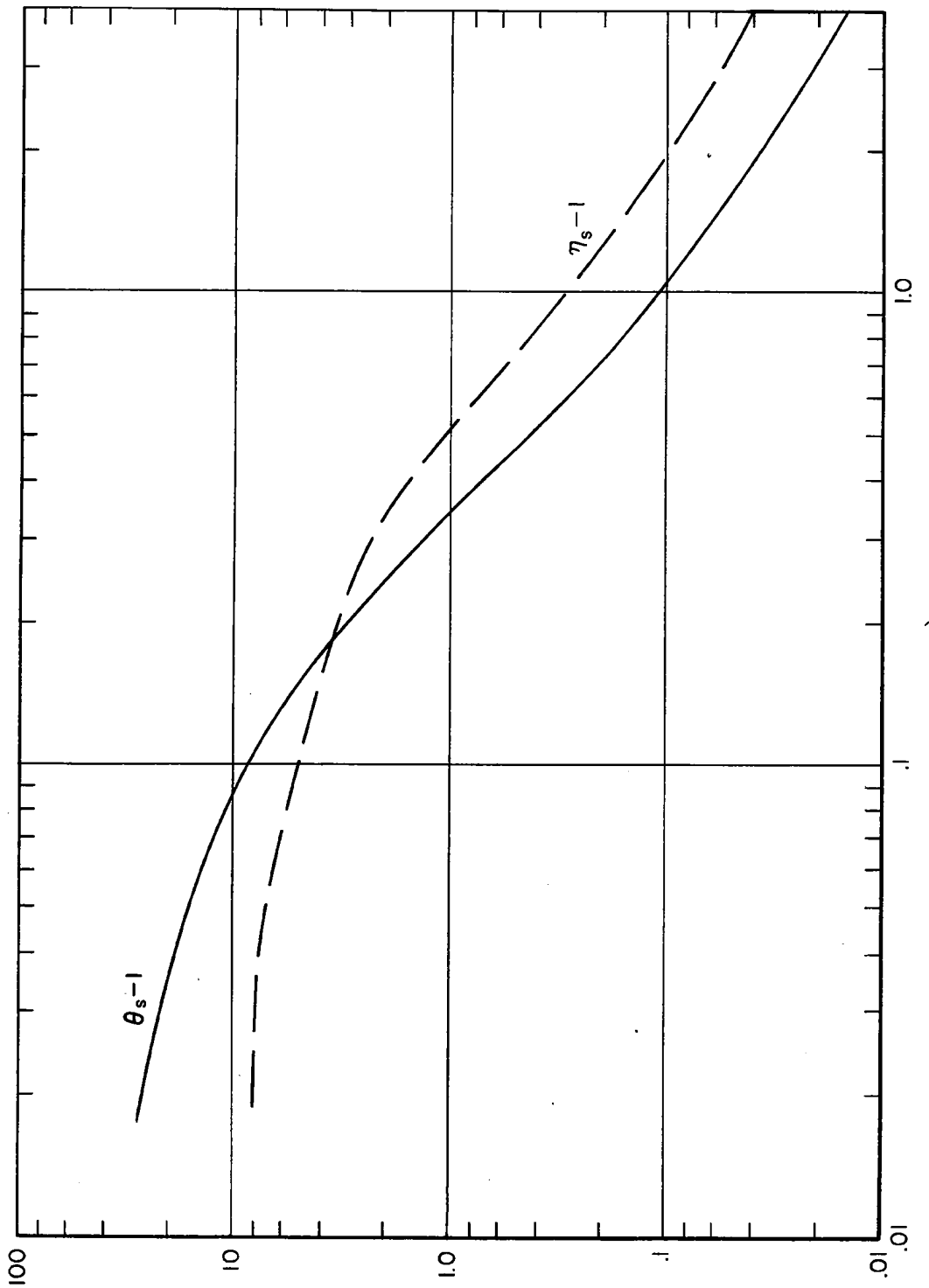

Fig. 3— Shock temperature (T_S °C / T_O °K = $\theta_S - 1$) and shock compression ($\rho_S / \rho_O - 1 = \eta_S - 1$) vs shock radius ($\lambda_S = R_S / a$) for TNT blast

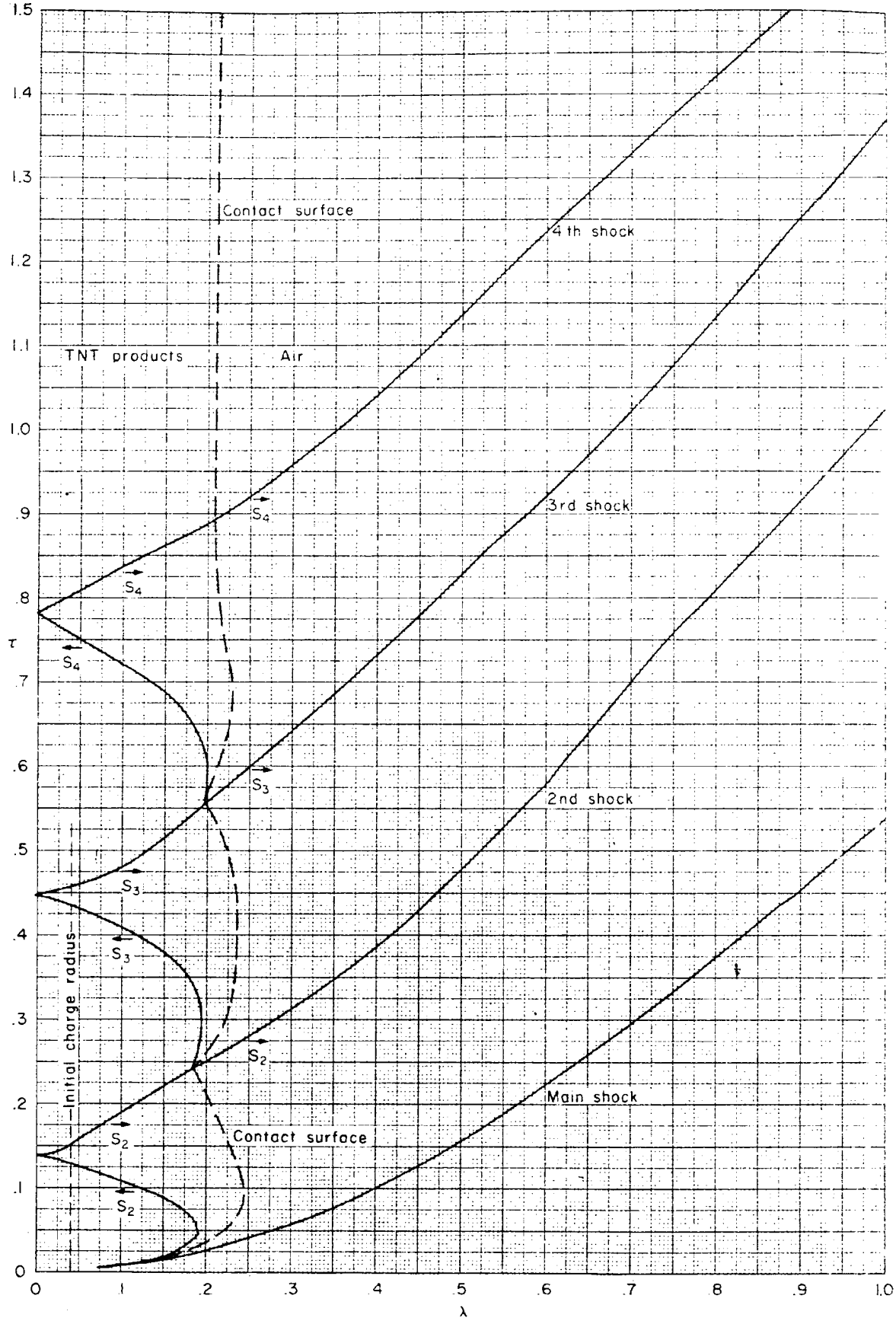

Fig. 4—Space-time diagram of shocks and contact surface for TNT blast

FIG. 5
DIVISION OF ENERGY BETWEEN KINETIC (Q) AND INTERNAL (E) TNT BLAST

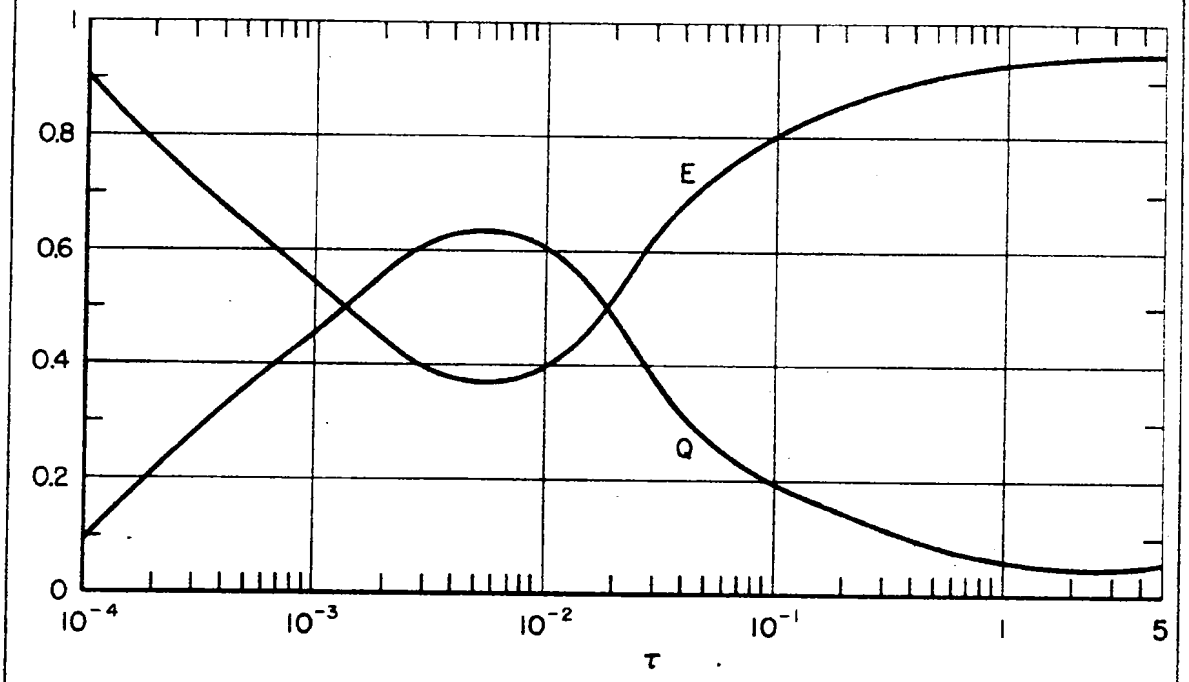

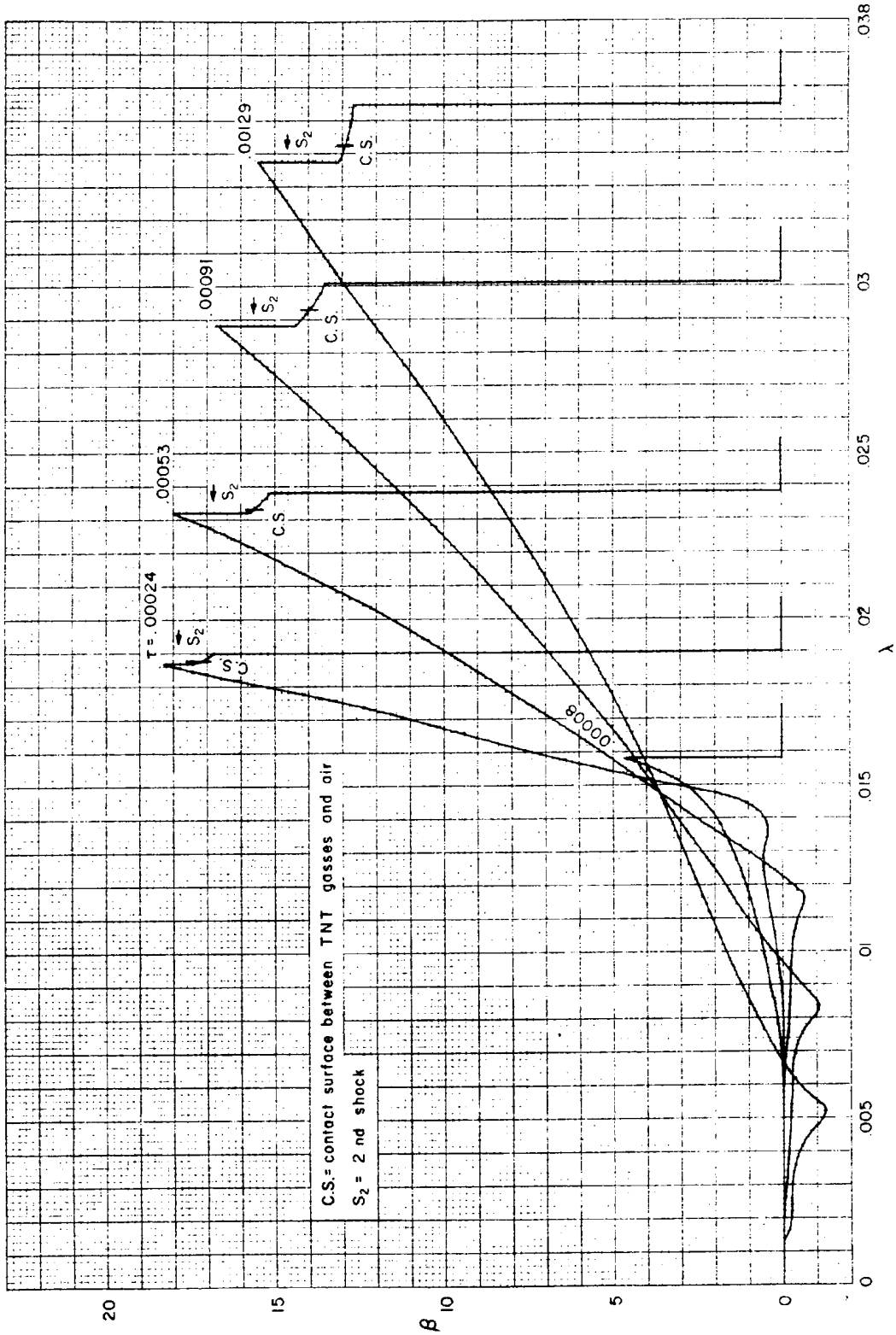

Fig. 6 — Particle velocity ($\beta = u/c_0$) vs radius ($\lambda = r/a$) at indicated times ($\tau = tc_0/a$) for a TNT blast

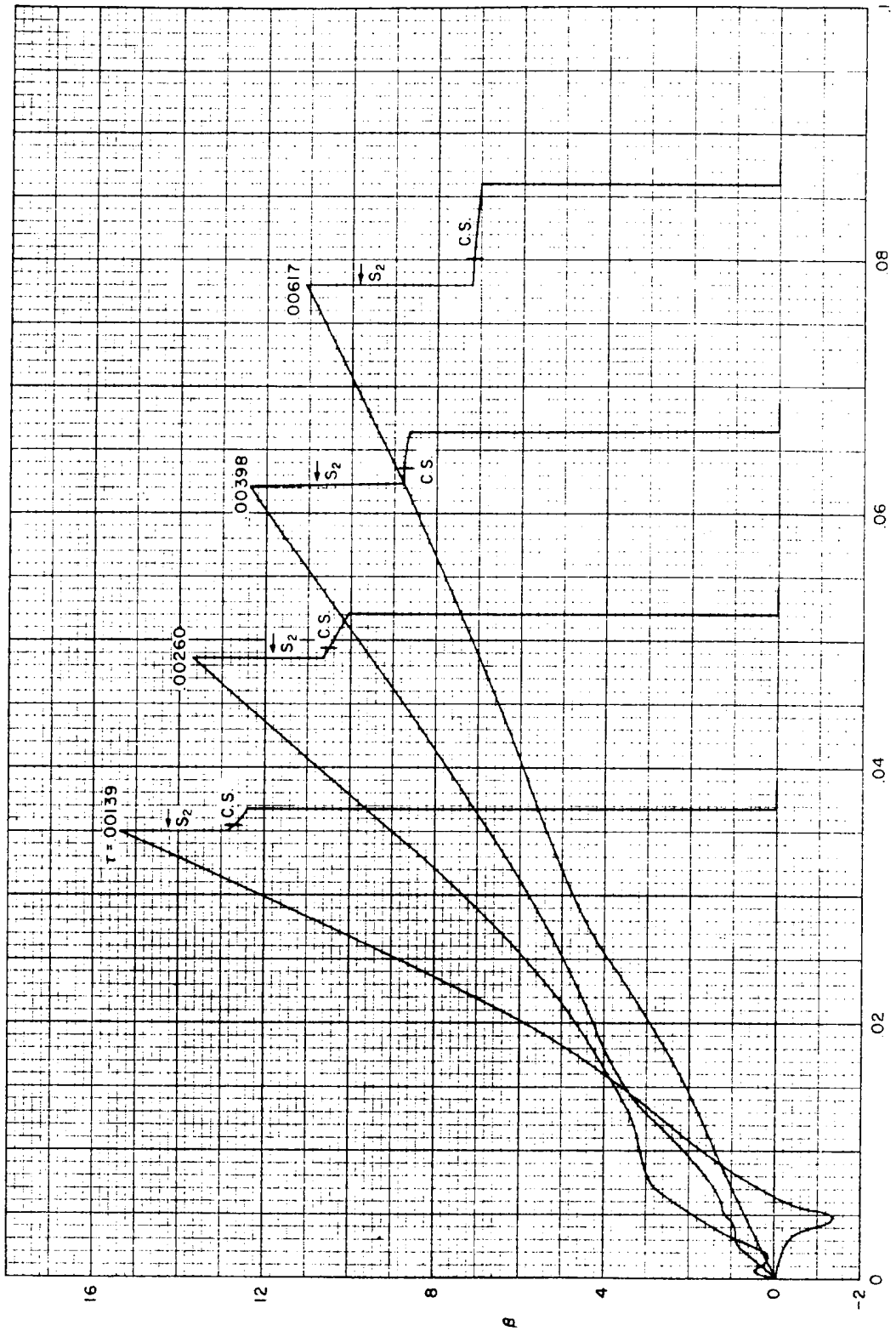

Fig. 7 — Particle velocity ($\beta = u/c_0$) vs radius ($\lambda = r/a$) at indicated times ($\tau = tc_0/a$) for a TNT blast

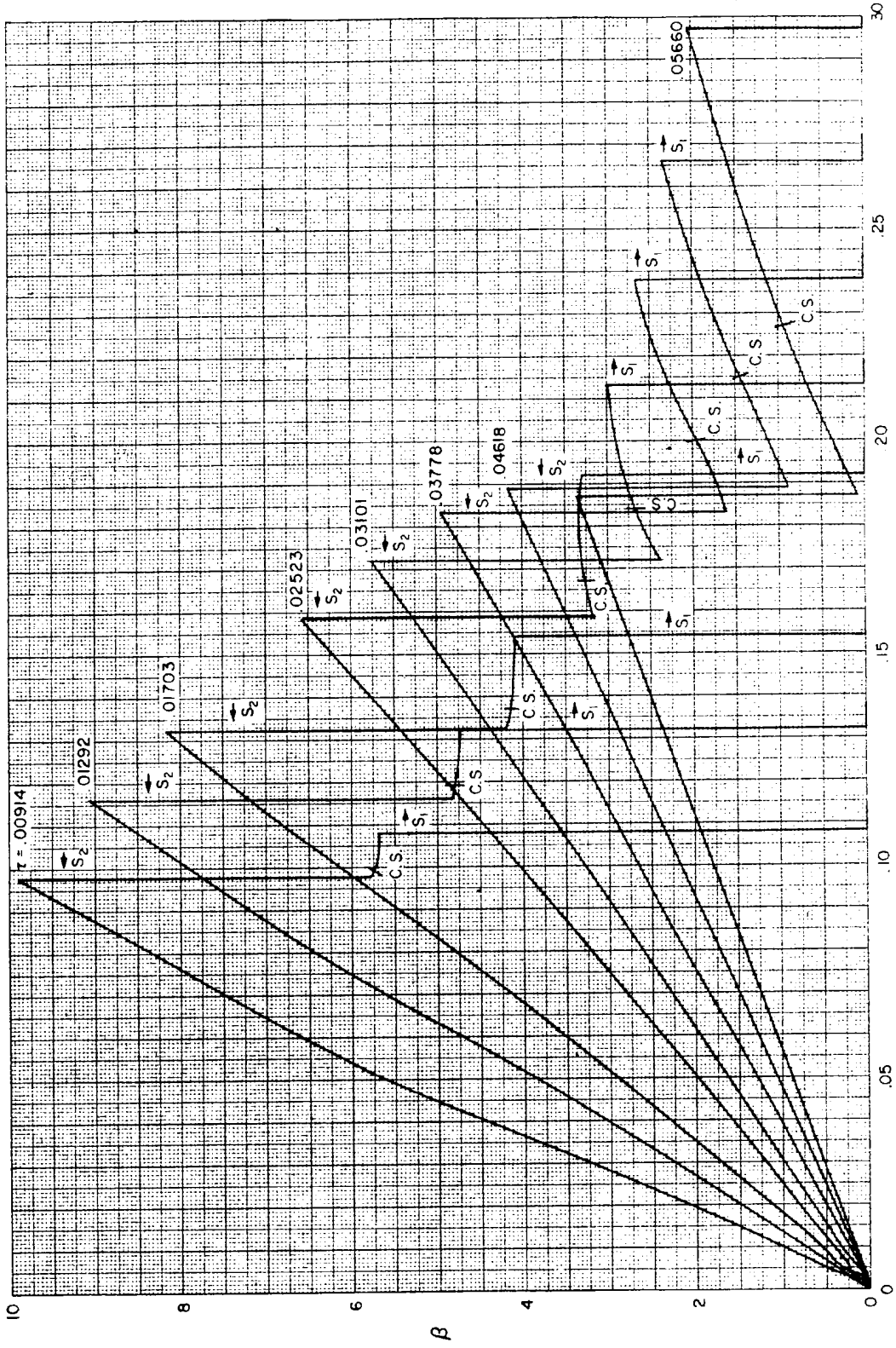

Fig. 8 — Particle velocity ($\beta = u/c_0$) vs radius ($\lambda = r/a$) at indicated times ($\tau = tc_0/a$) for a TNT blast

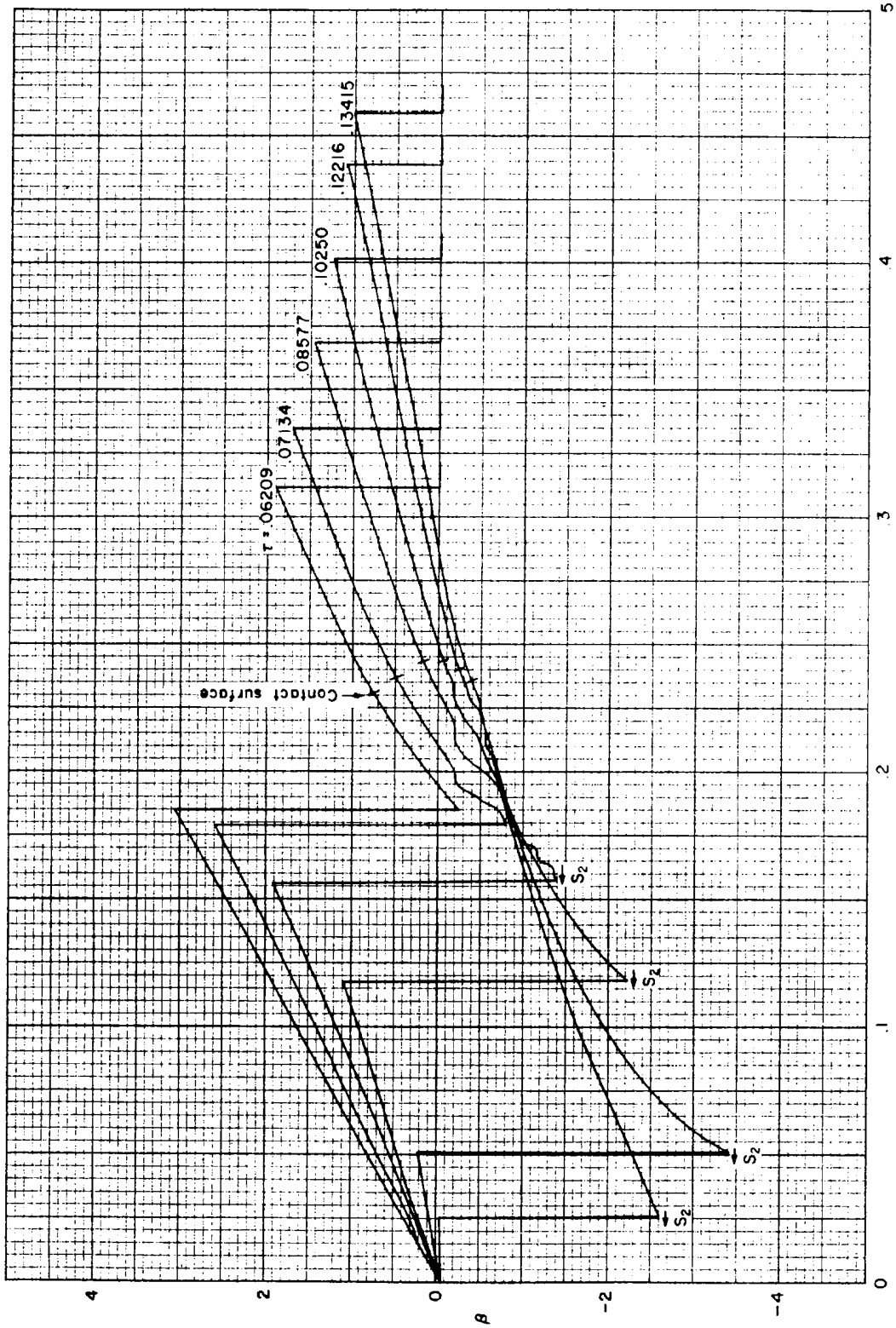

Fig. 9—Particle velocity ($\beta = u/c_0$) vs radius ($\lambda = r/a$) at indicated times ($\tau = tc_0/a$) for a TNT blast

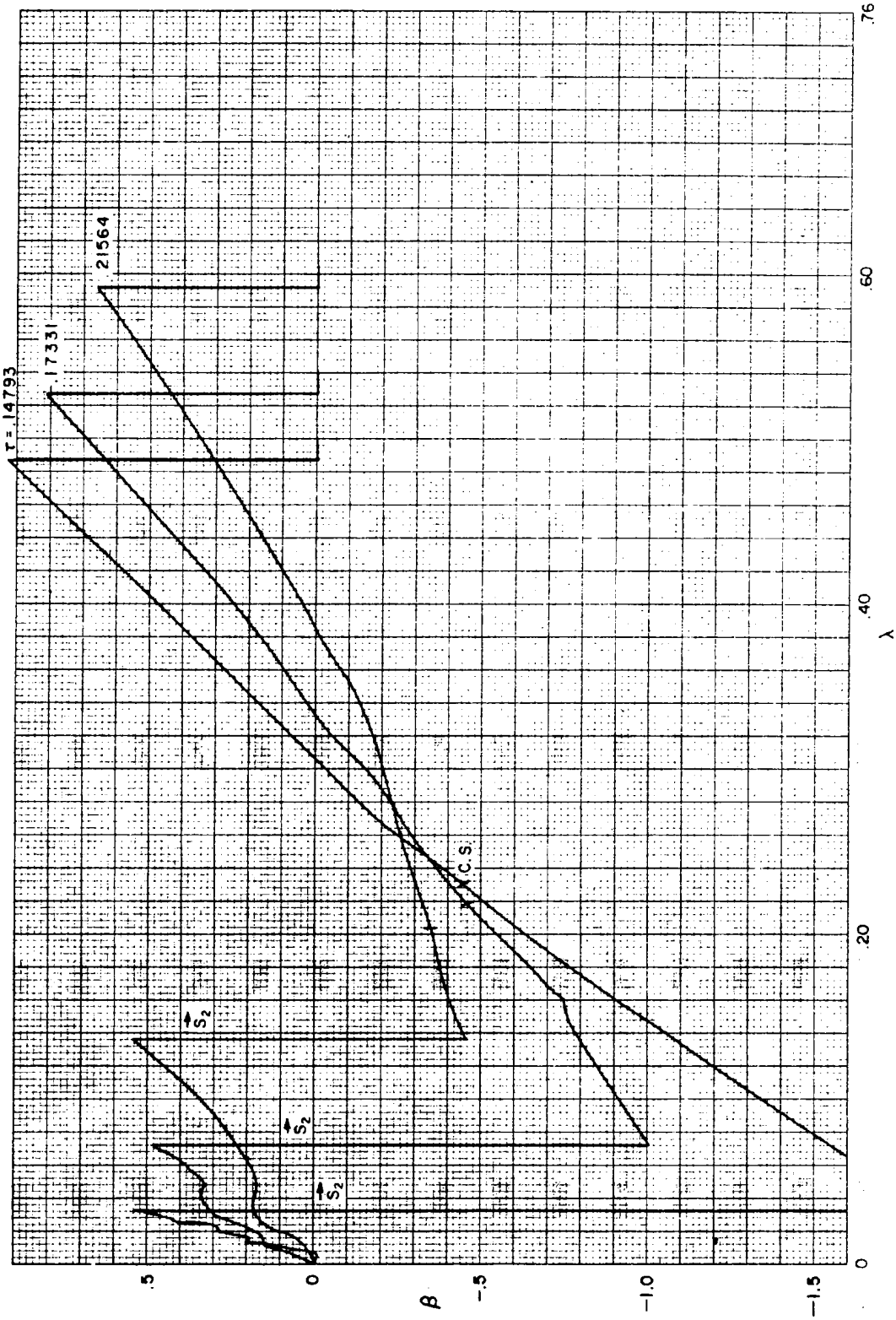

Fig. 10 — Particle velocity ($\beta = u/c_0$) vs radius ($\lambda = r/a$) at indicated times ($\tau = tc_0/a$) for a TNT blast

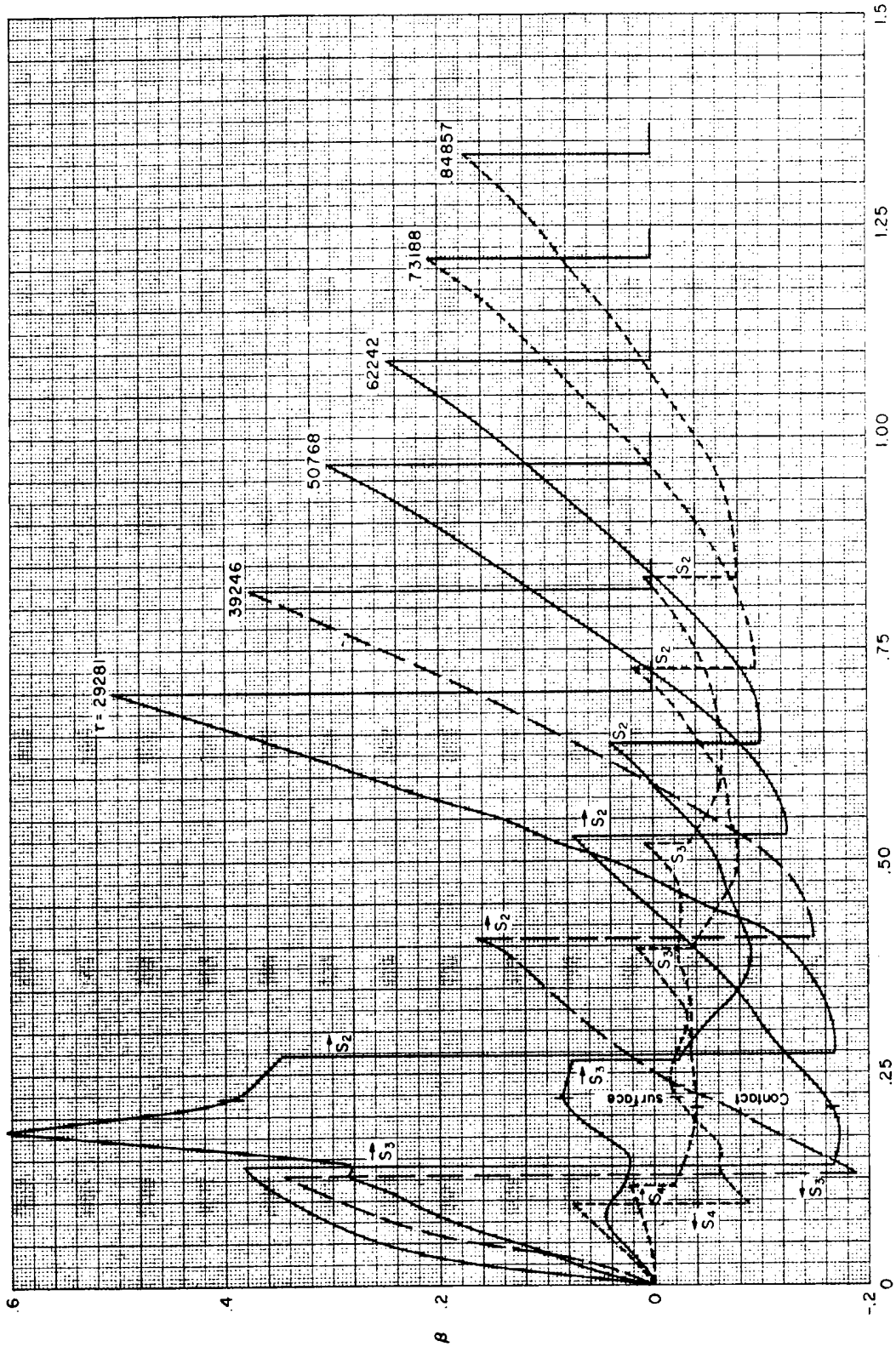

Fig.11—Particle velocity ($\beta = u/c_0$) vs radius ($\lambda = r/a$) at indicated times ($\tau = tc_0/a$) for a TNT blast

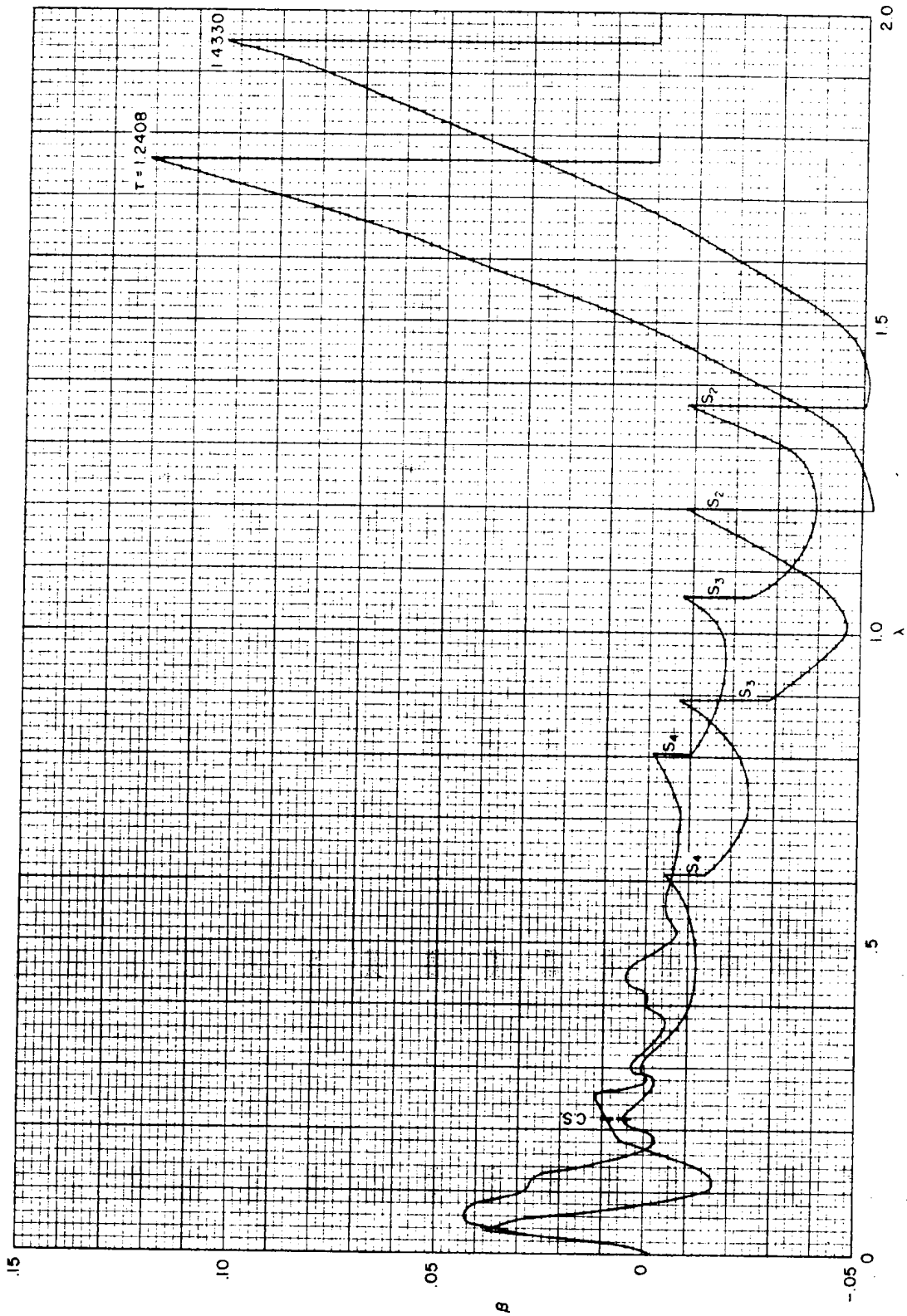

Fig.12—Particle velocity ($\beta = u/c_0$) vs radius ($\lambda = r/a$) at indicated times ($\tau = tc_0/a$) for a TNT blast

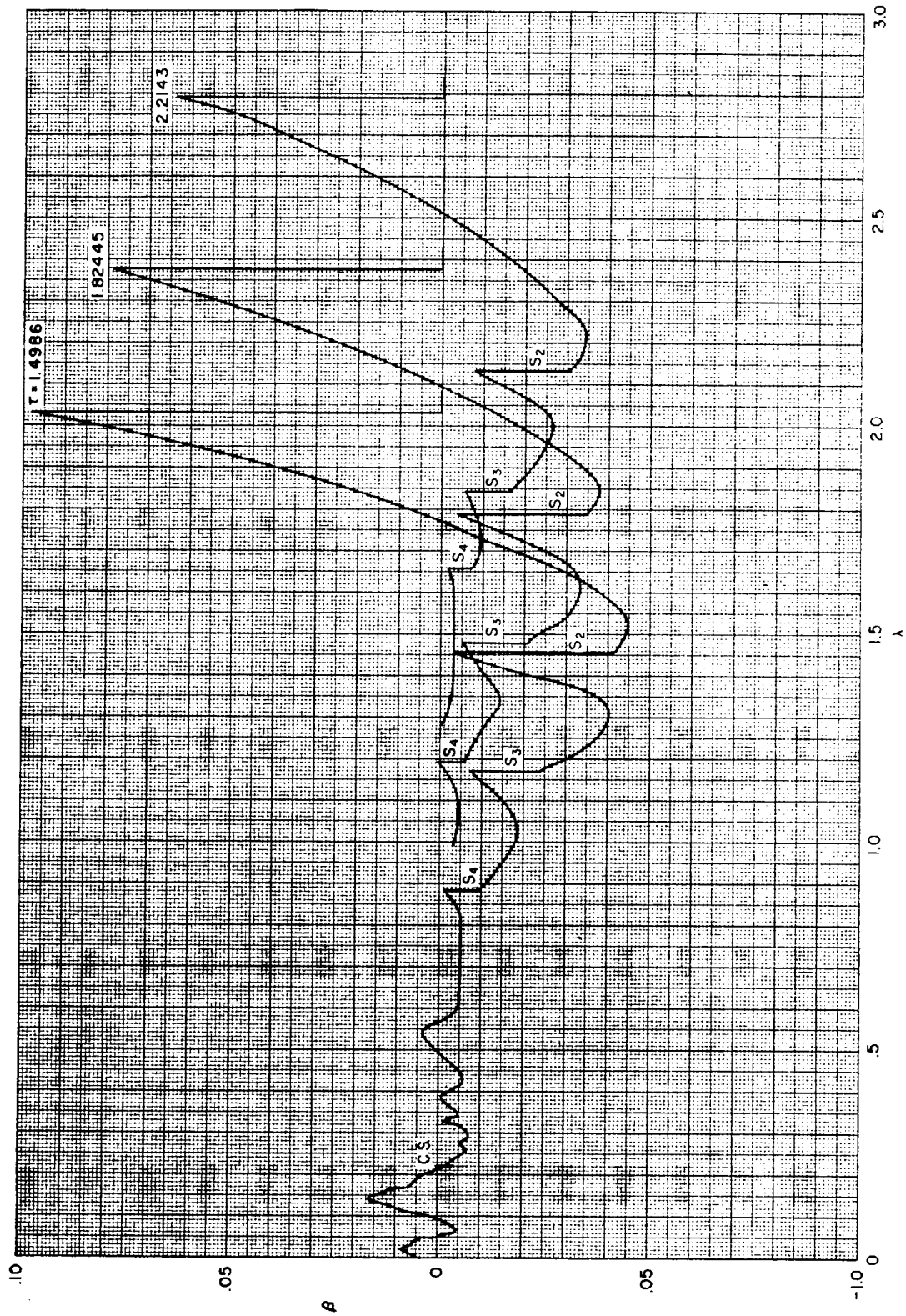

Fig.13—Particle velocity ($\beta = u/c_0$) vs radius ($\lambda = r/a$) at indicated times ($\tau = tc_0/a$) for a TNT blast

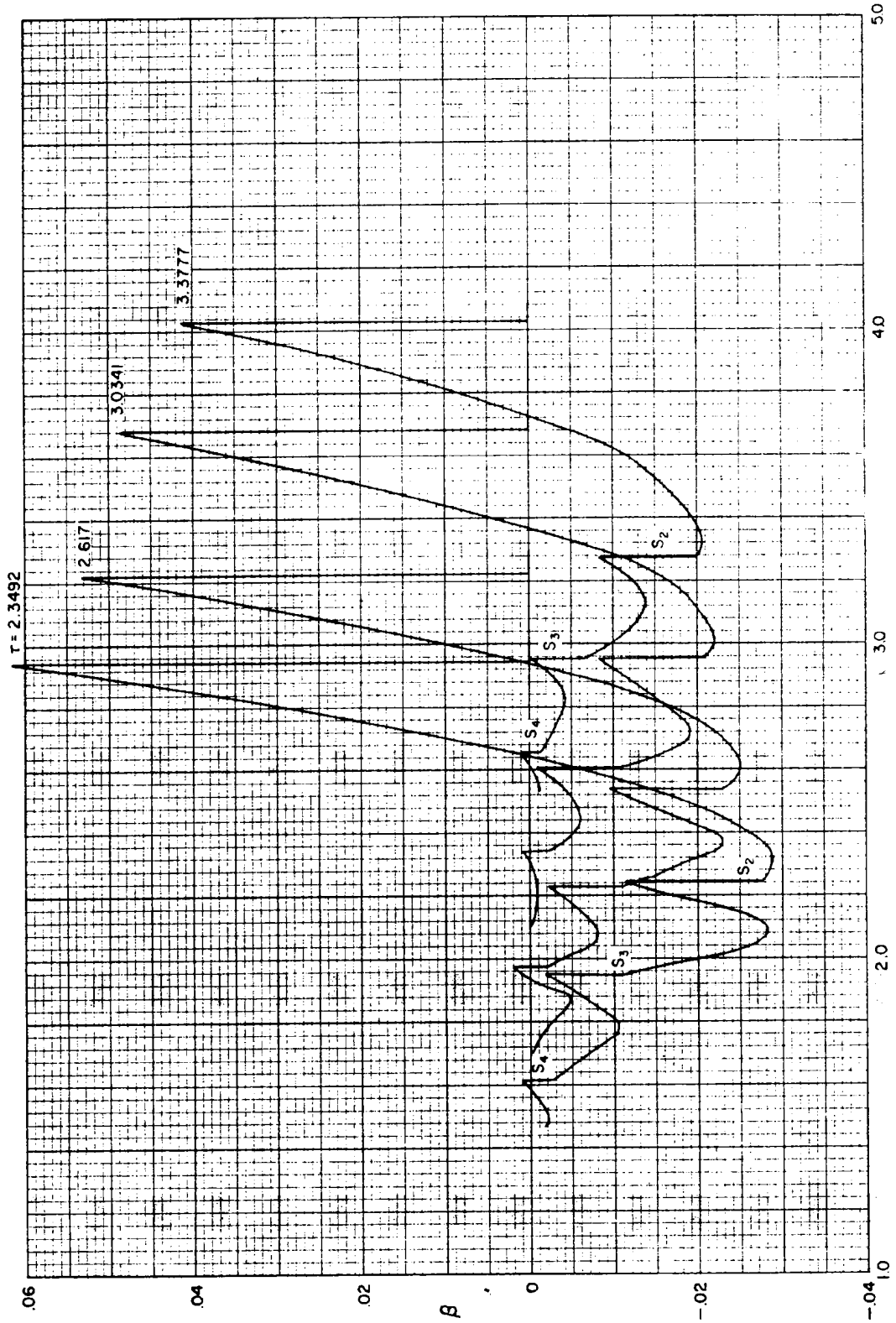

Fig. 14 — Particle velocity ($\beta = u/c_0$) vs radius ($\lambda = r/a$) at indicated times ($\tau = tc_0/a$) for a TNT blast

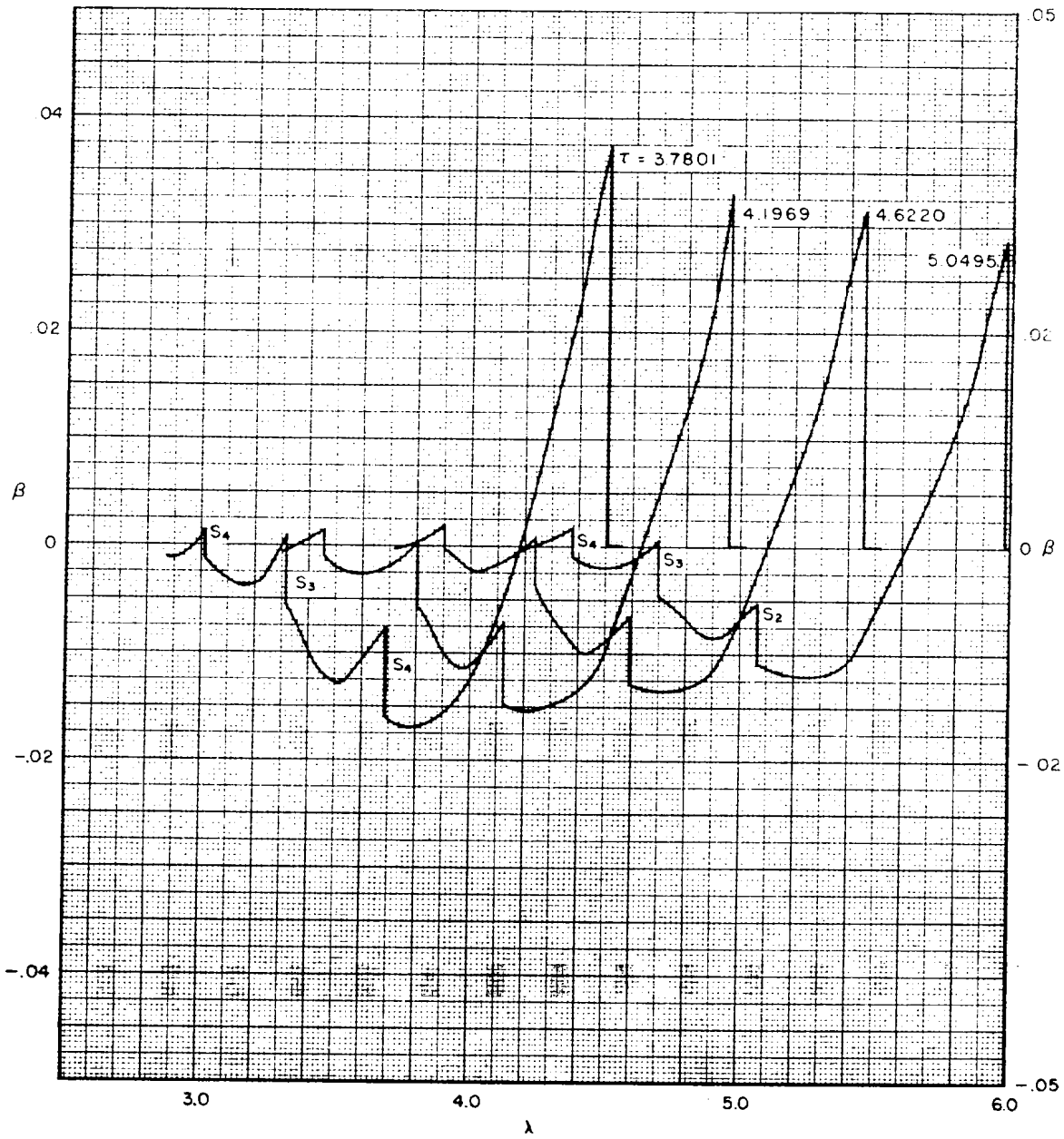

Fig. 15 — Particle velocity ($\beta = u/c_0$) vs radius ($\lambda = r/a$) as indicated times ($\tau = tc_0/a$) for a TNT blast

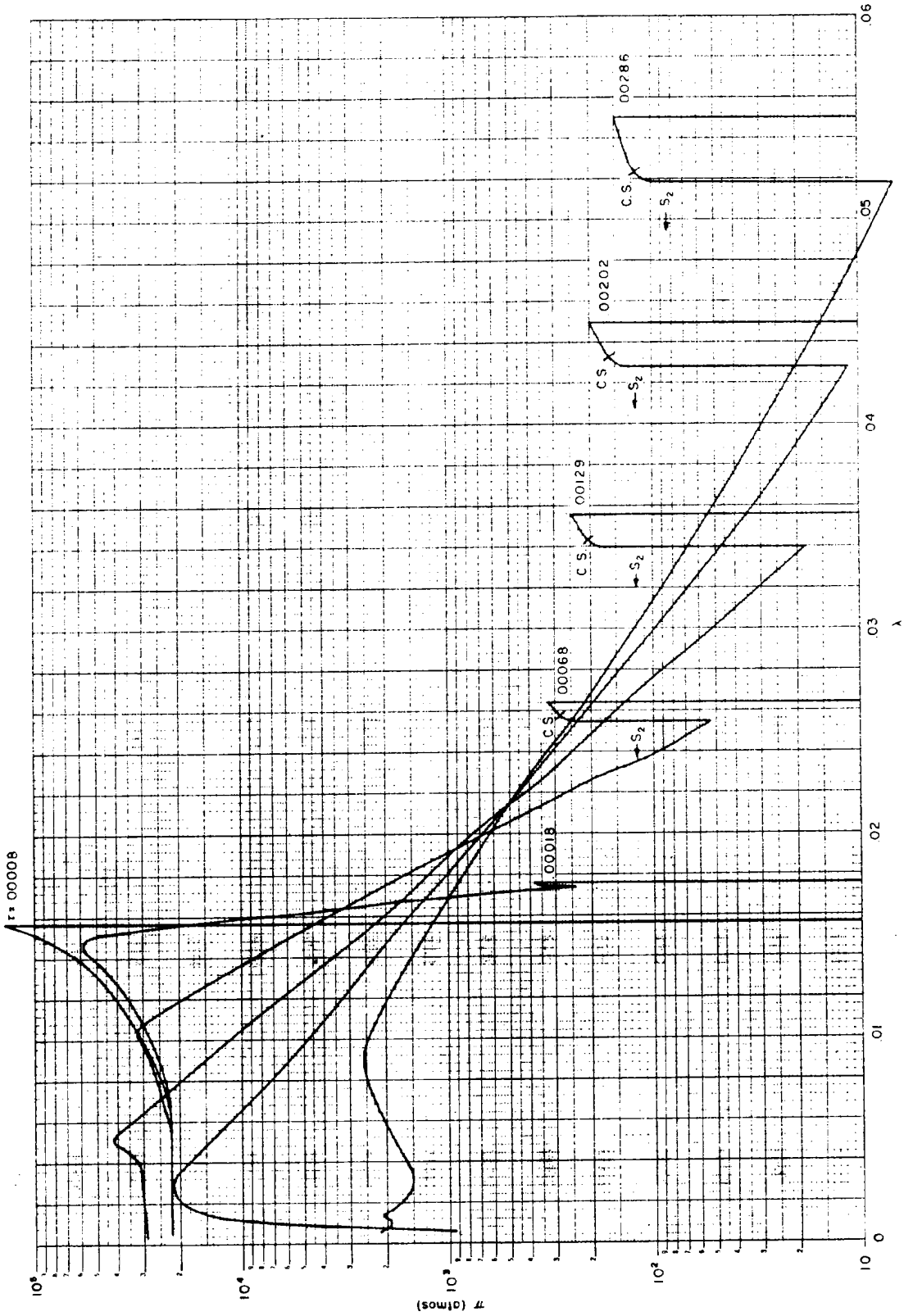

Fig. 16 – Pressure ($\pi = p/p_0$) vs radius ($\lambda = r/a$) at indicated times ($t = t_{sec}/a$) for a TNT blast

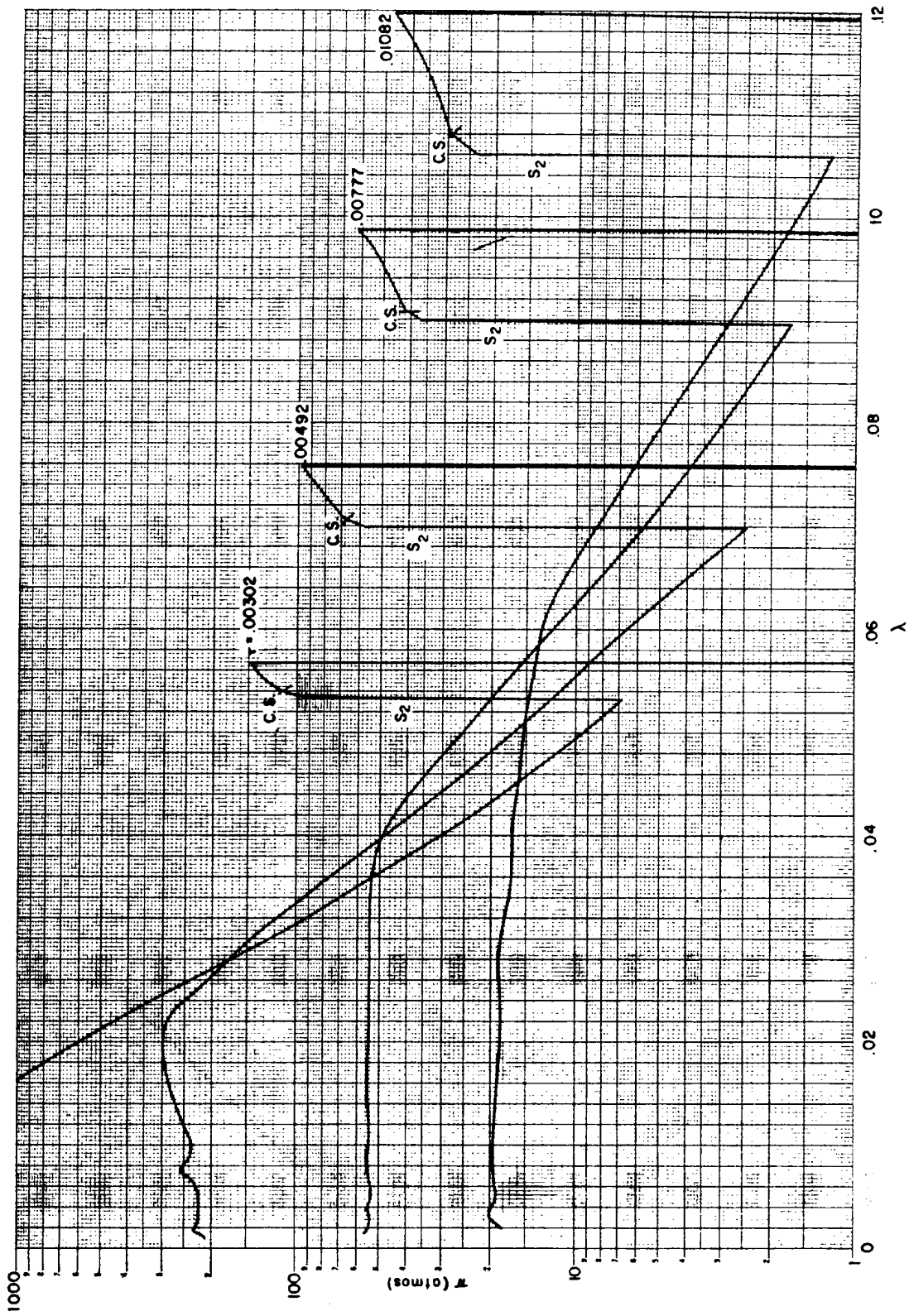

Fig. 17—Pressure ($\pi = p/p_0$) vs. radius ($\lambda = r/a$) at indicated times ($\tau = tc_0/a$) for a TNT blast

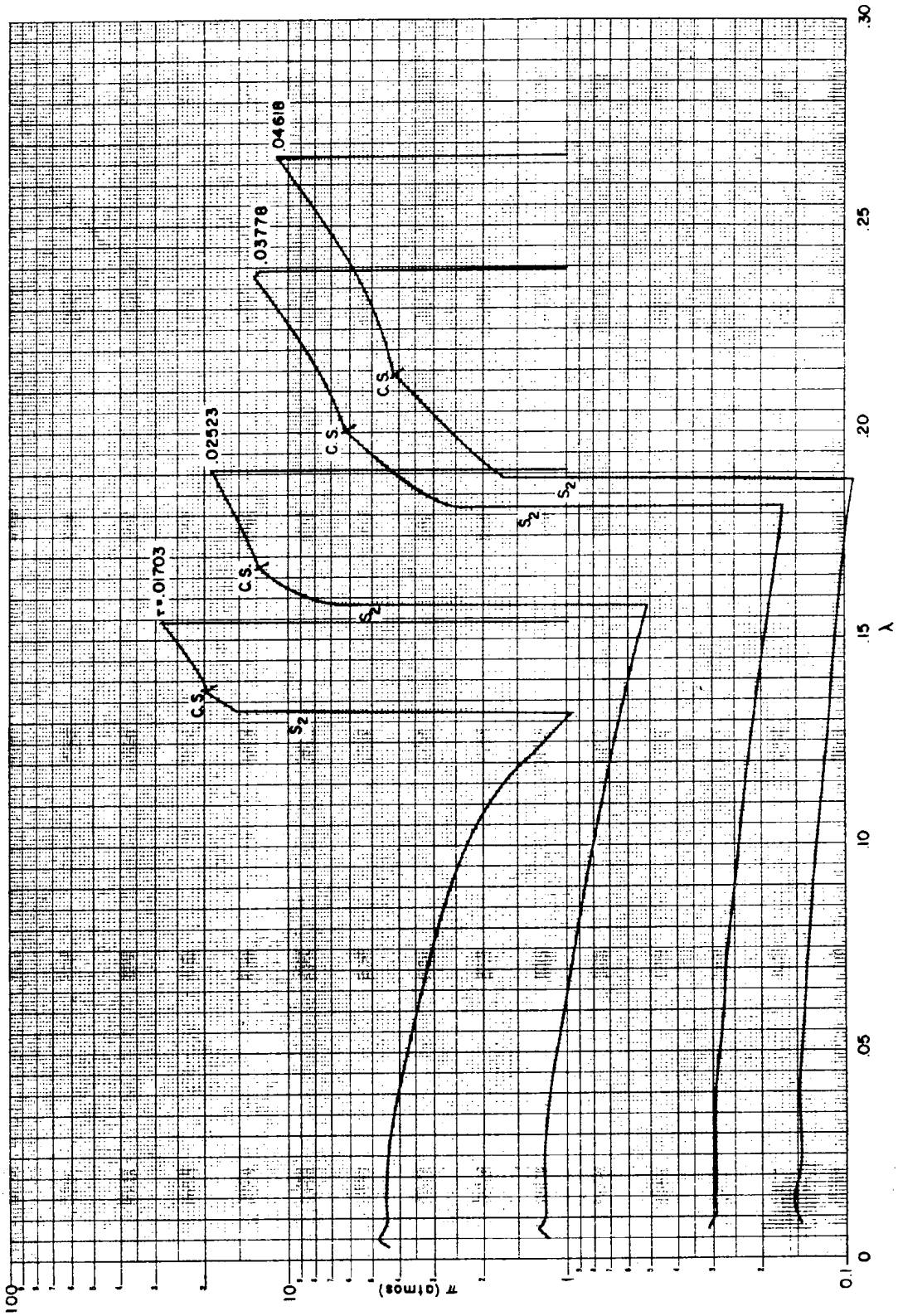

Fig. 18– Pressure ($\pi = p/p_0$) vs. radius ($\lambda = r/a$) at indicated times ($\tau = tc_0/a$) for a TNT blast

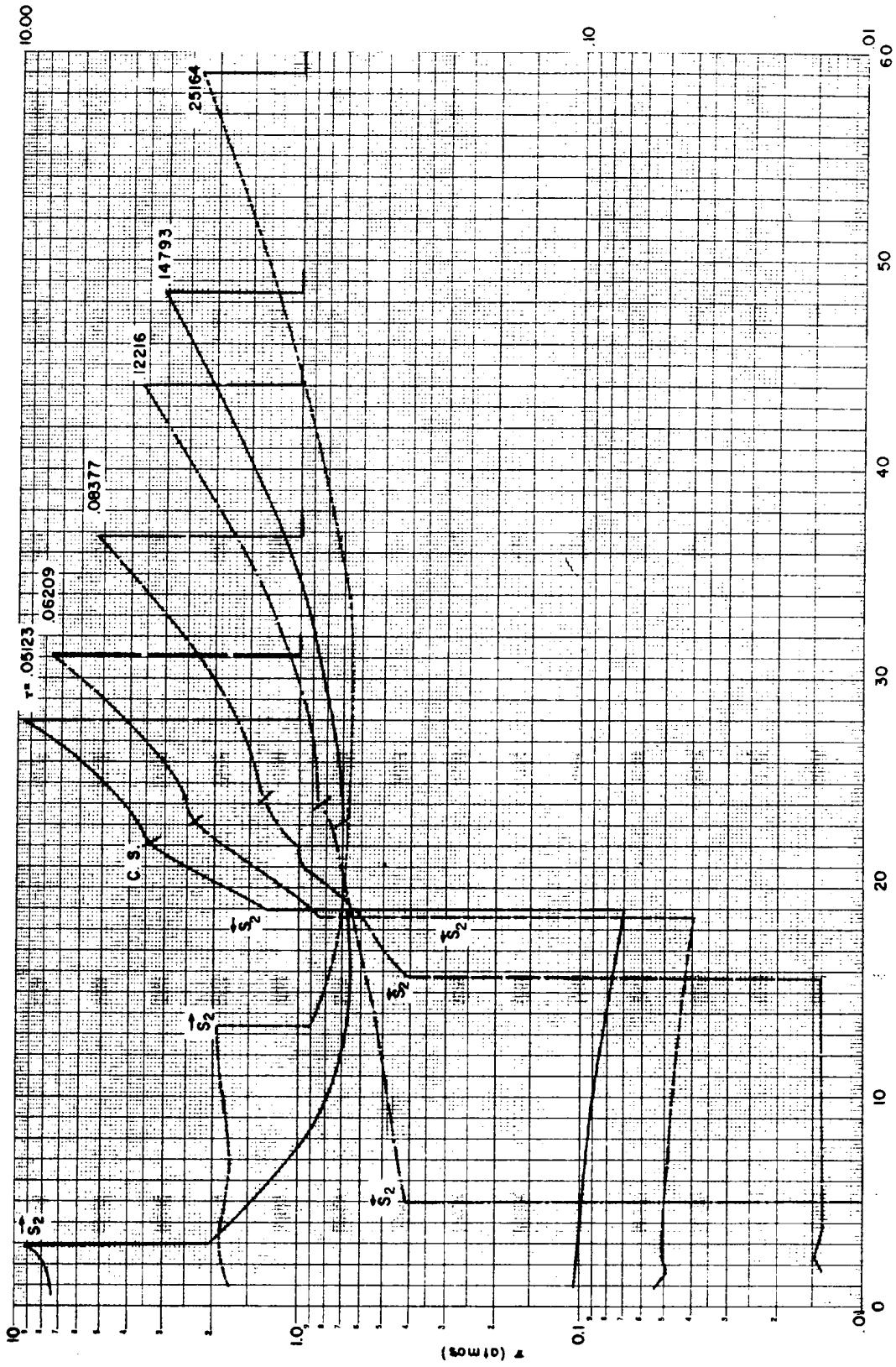

Fig. 19— Pressure ($\pi = p/p_0$) vs. radius ($\lambda = r/a$) at indicated times ($\tau = tc_0/a$) for a TNT blast

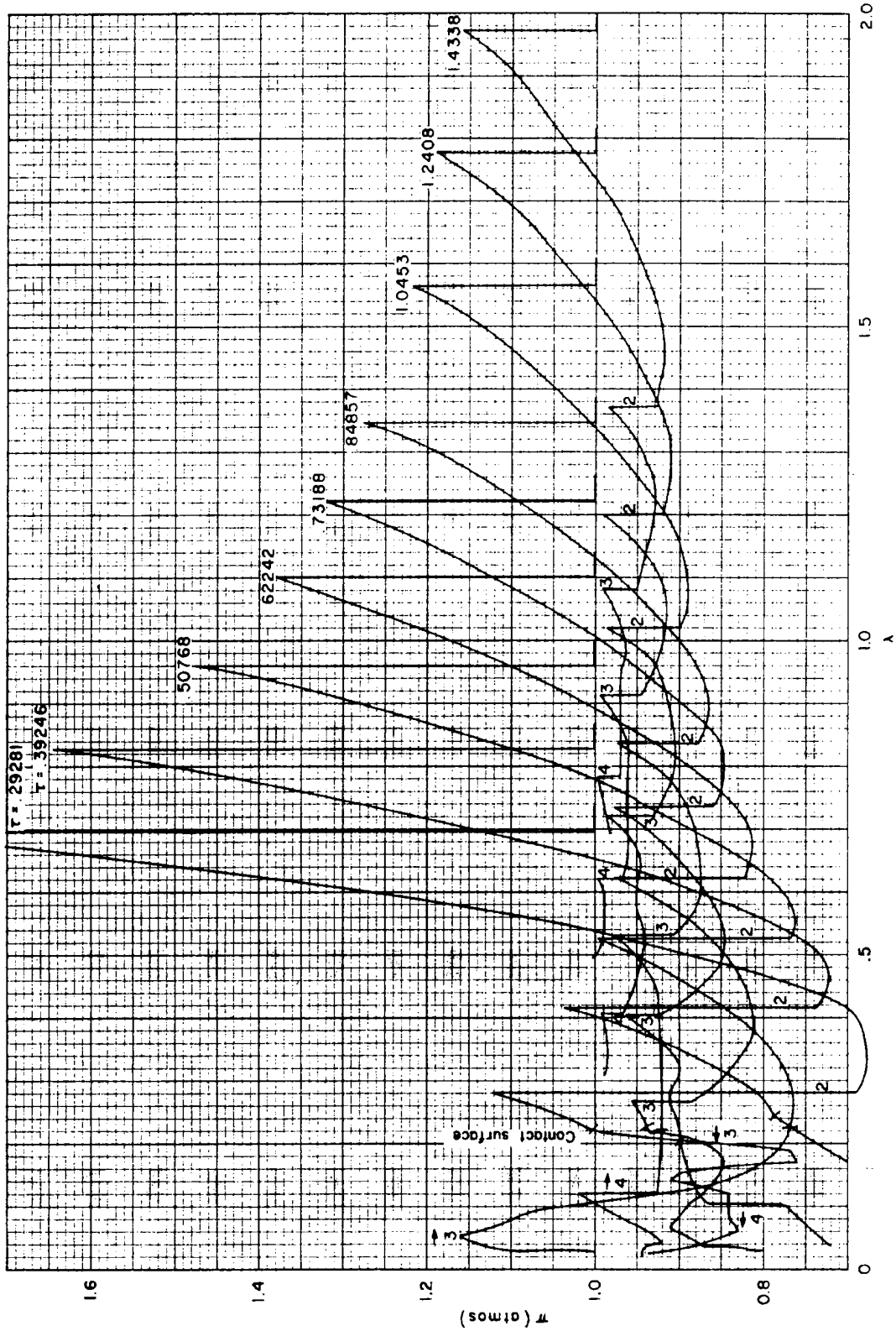

Fig. 20—Pressure ($\pi = p/p_0$) vs radius ($\lambda = r/a$) at indicated times ($\tau = tc_0/a$) for a TNT blast

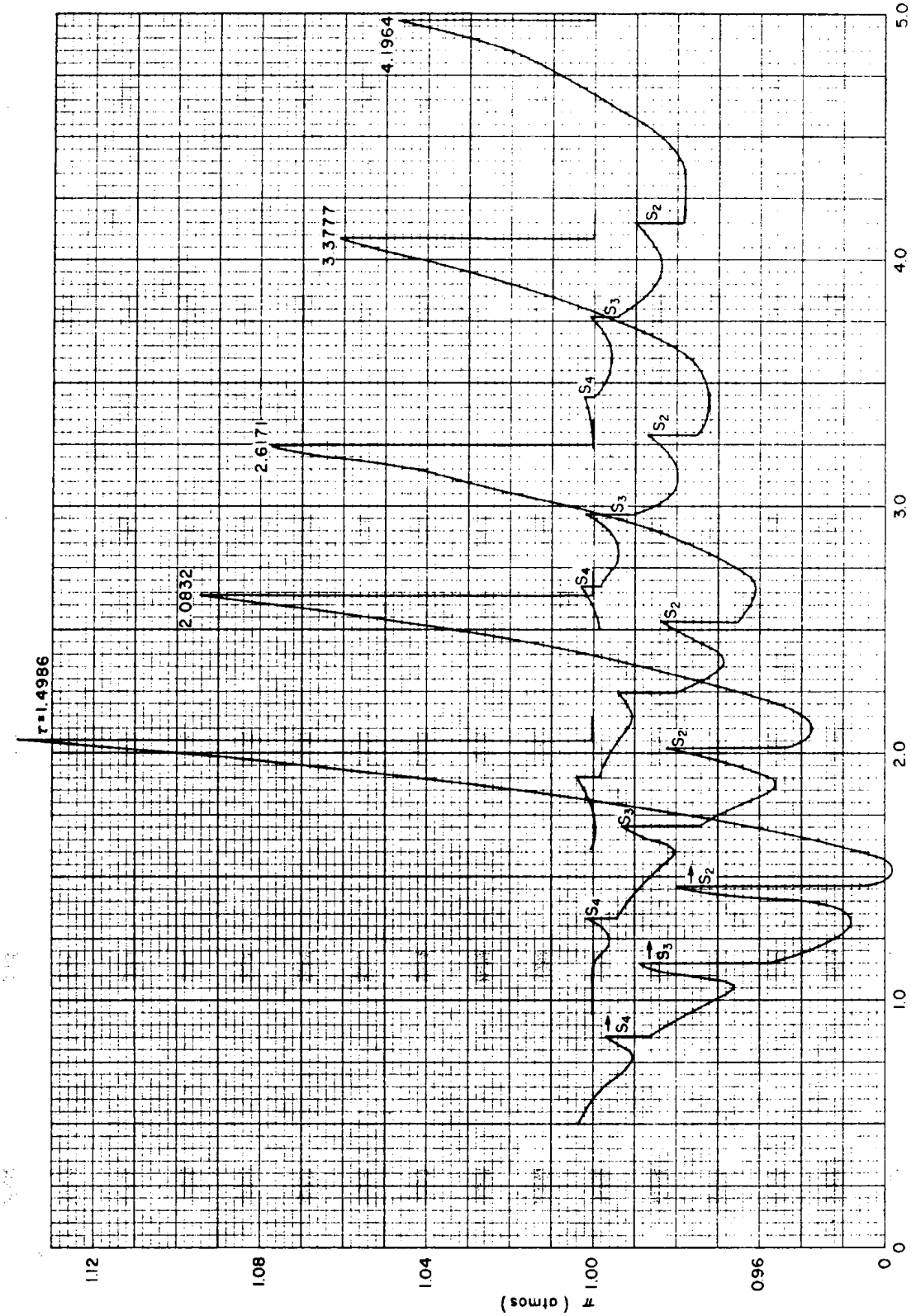

Fig. 21—Pressure ($\pi=p/p_0$) vs radius ($\lambda=r/a$) at indicated times ($\tau=tc_0/a$) for a TNT blast

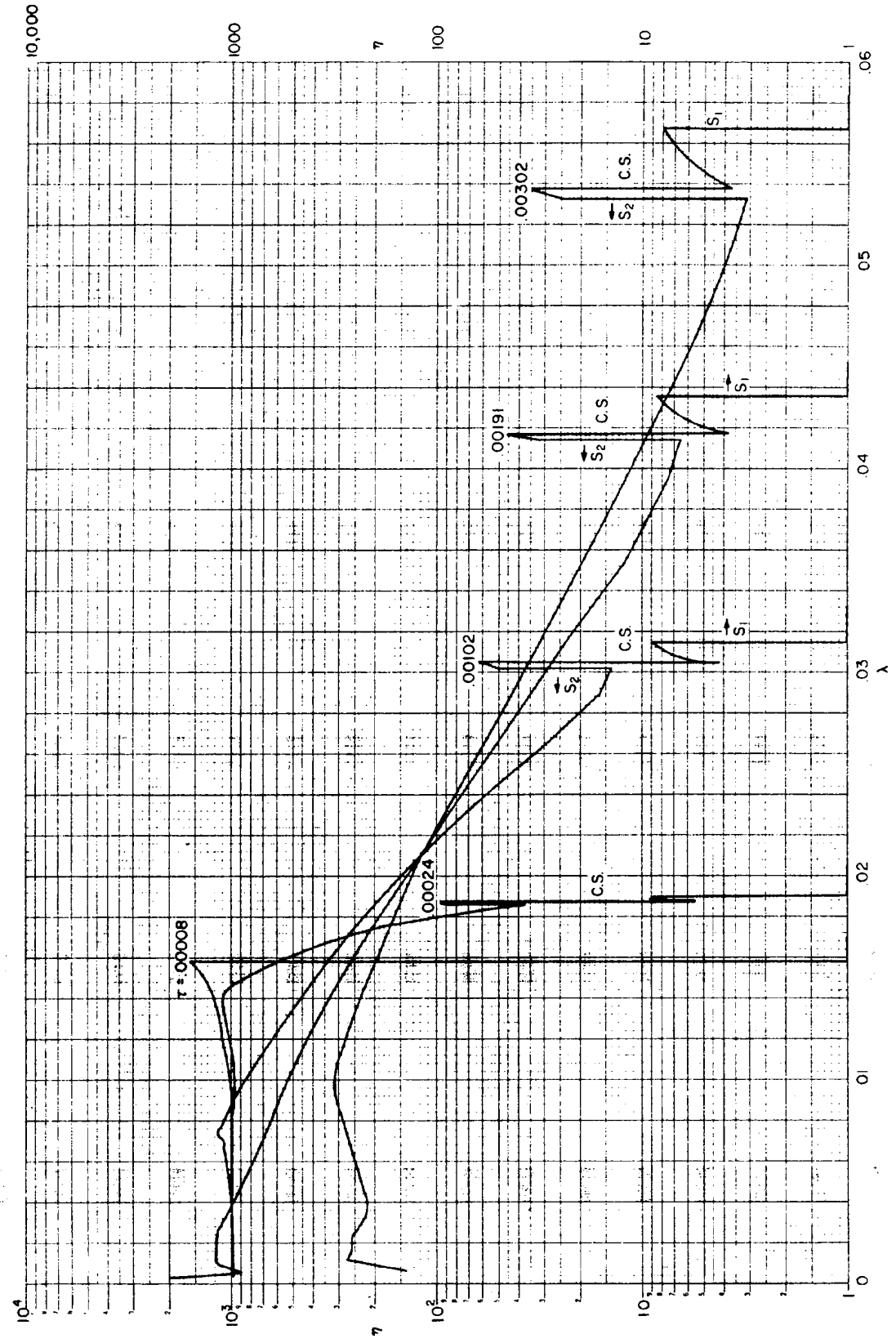

Fig. 22 — Density ($\eta = \rho/\rho_0$) vs radius ($\lambda = r/a$) at indicated times ($\tau = tc_0/a$) for a TNT blast

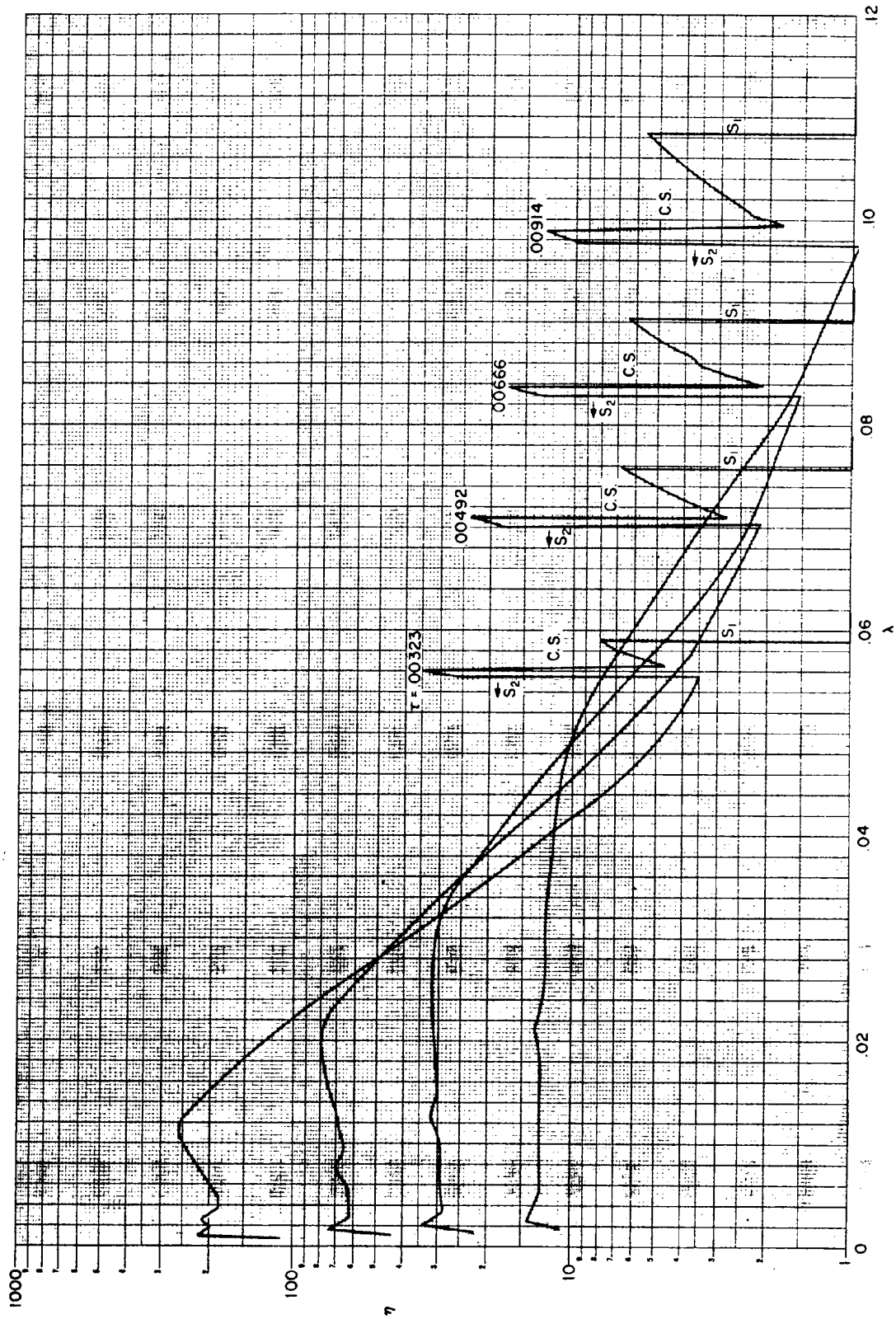

Fig. 23— Density ($\eta = \rho/\rho_0$) vs radius ($\lambda = r/a$) at indicated times ($\tau = tc_0/a$) for a TNT blast

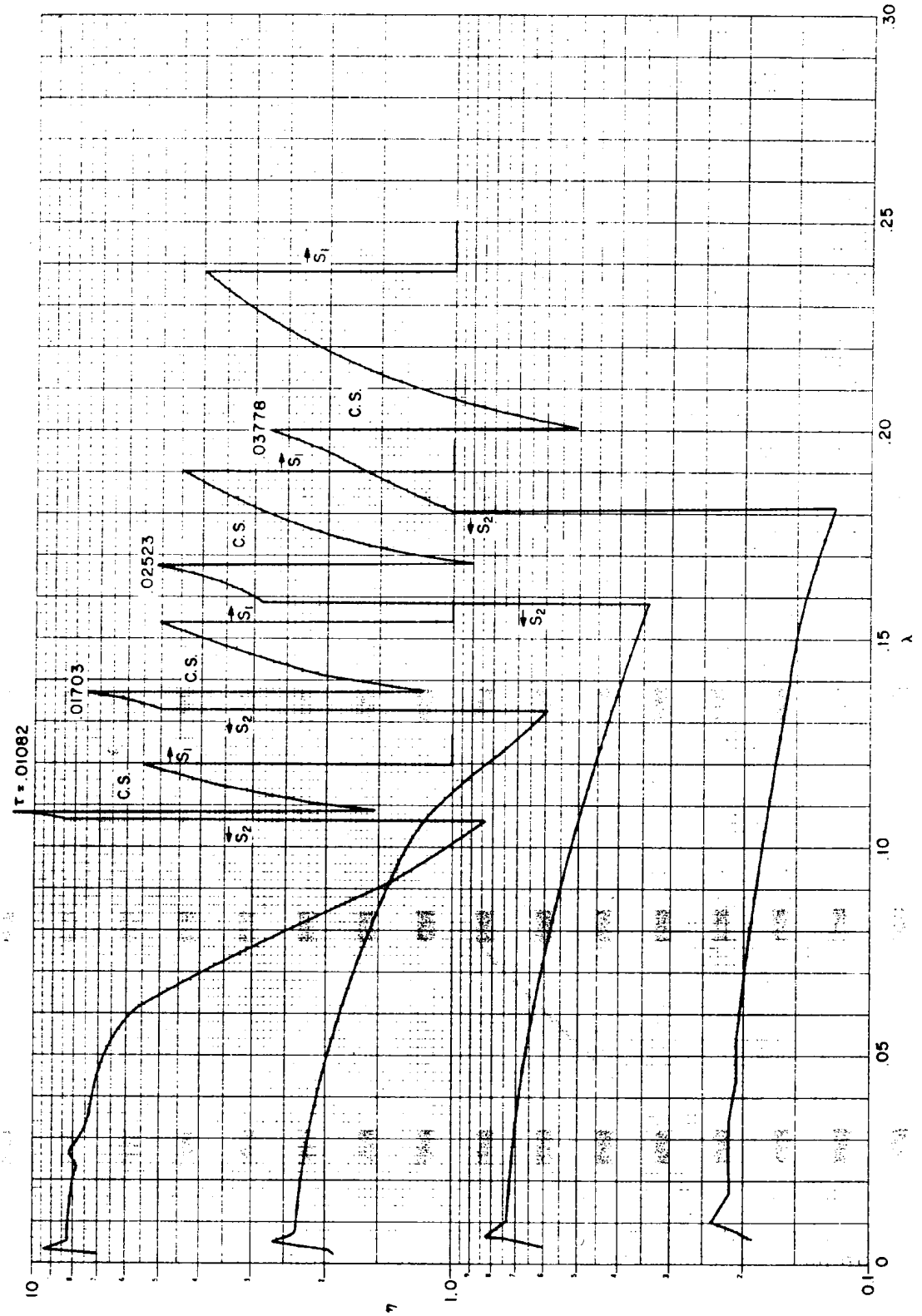

Fig. 24 — Density ($\eta = \rho/\rho_0$) vs radius ($\lambda = r/a$) at indicated times ($\tau = tc_0/a$) for a TNT blast

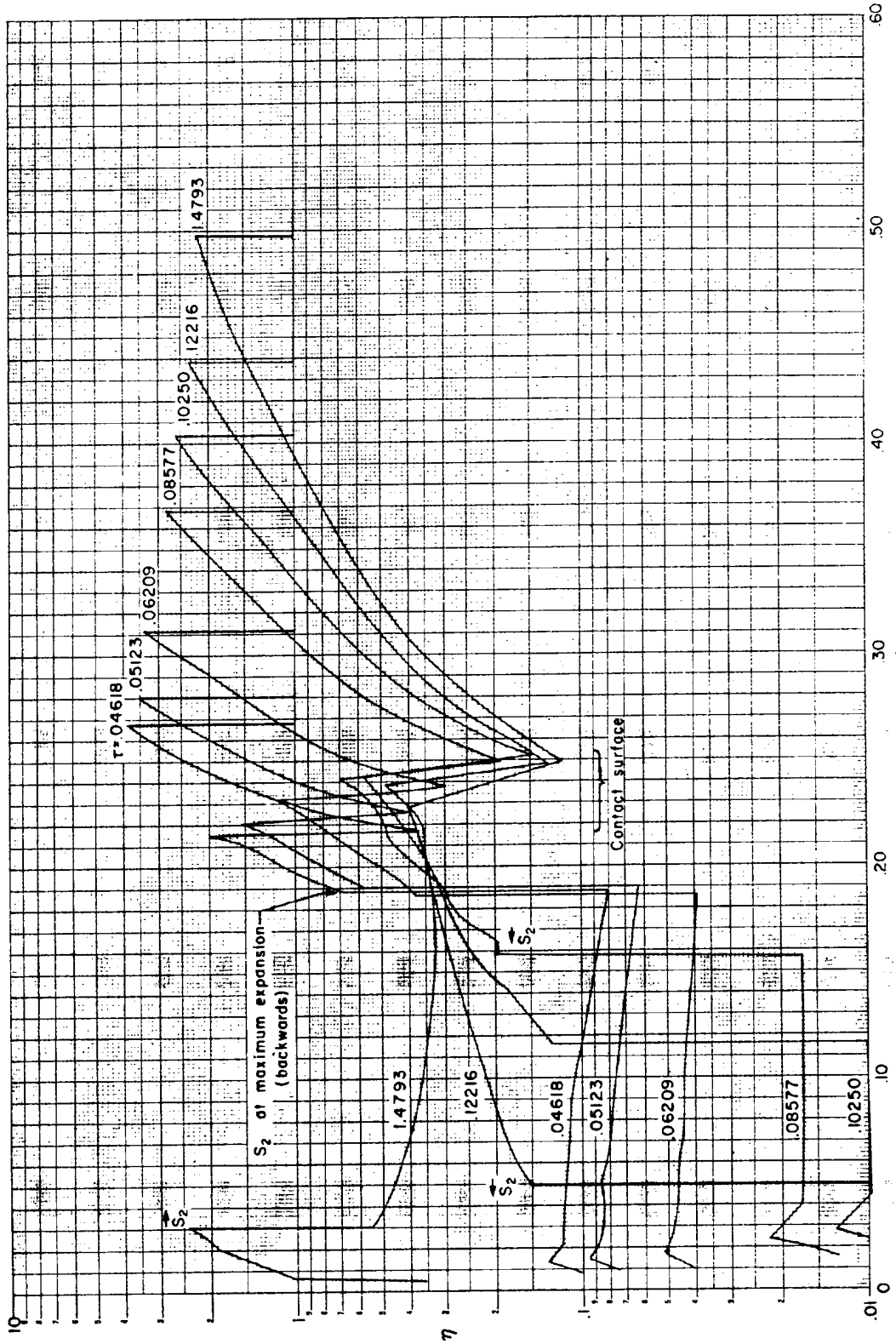

Fig.25—Density ($\eta = \rho/\rho_0$) vs radius ($\lambda = r/a$) at indicated times ($\tau = tc_0/a$) for a TNT blast

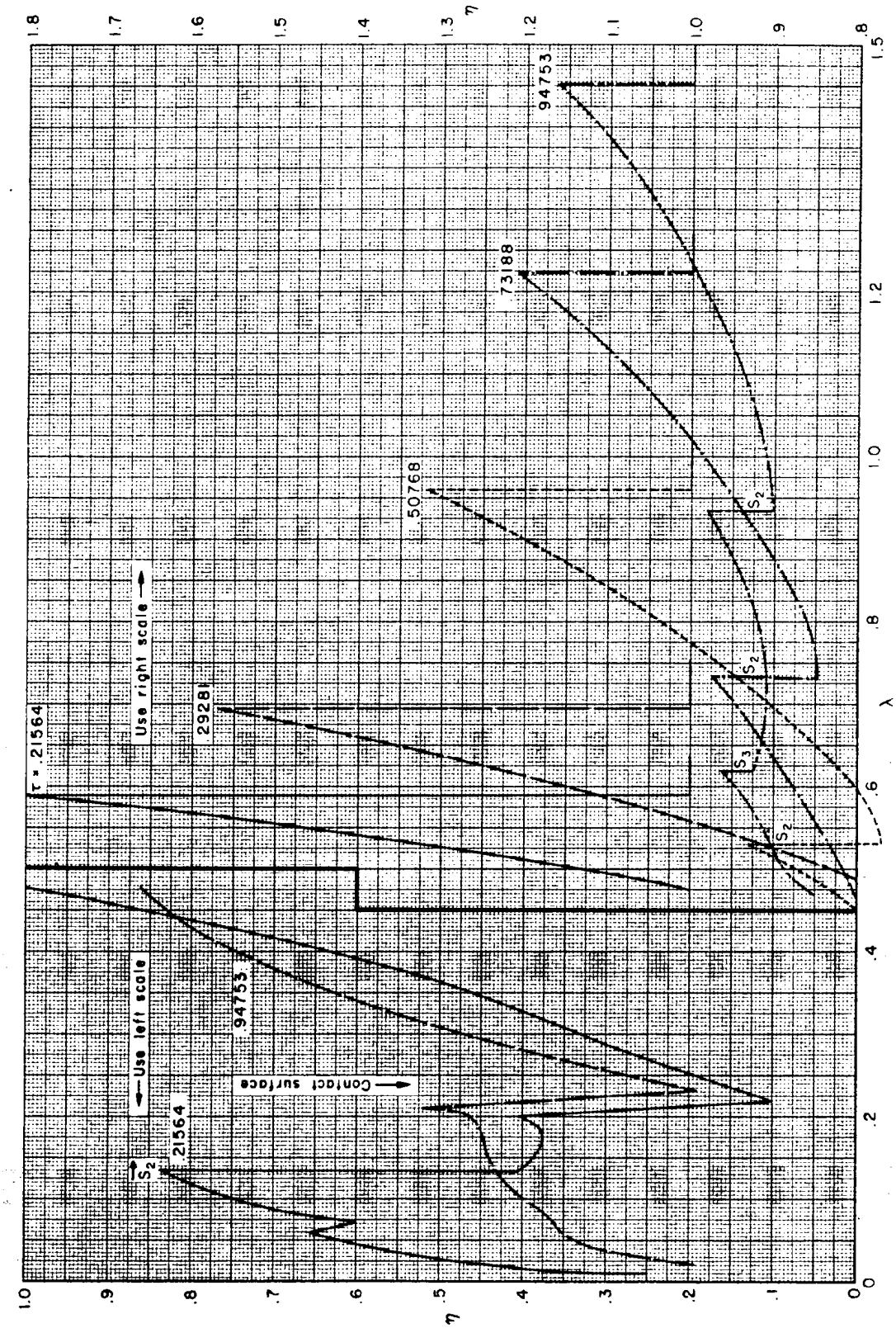

Fig. 26—Density ($\eta = \rho/\rho_0$) vs radius ($\lambda = r/a$) at indicated times ($\tau = \tau c_0/a$) for a TNT blast

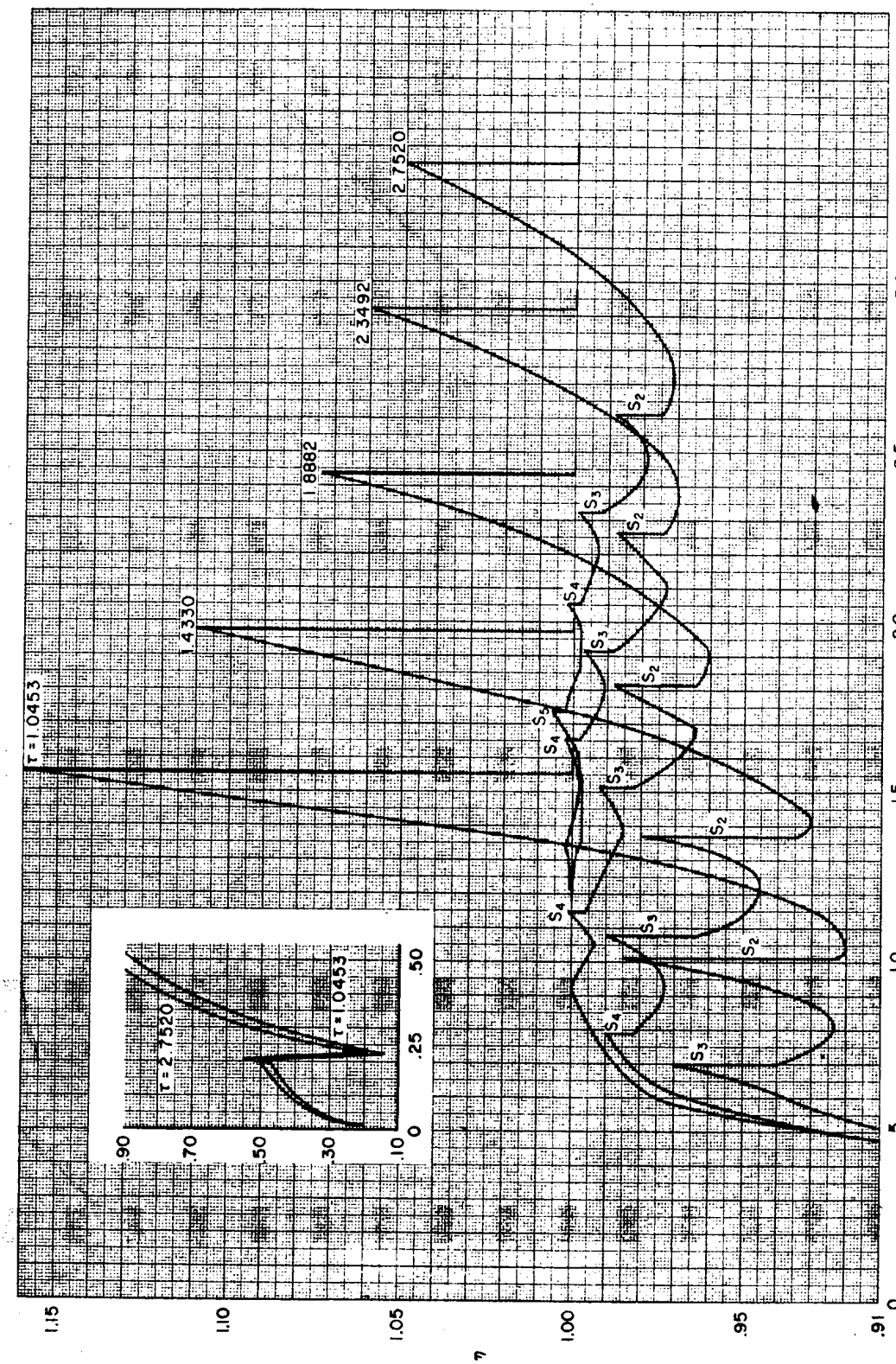

Fig. 27—Density ($\eta = \rho/\rho_0$) vs radius ($\lambda = r/a$) at indicated times ($\tau = tc_0/a$) for a TNT blast

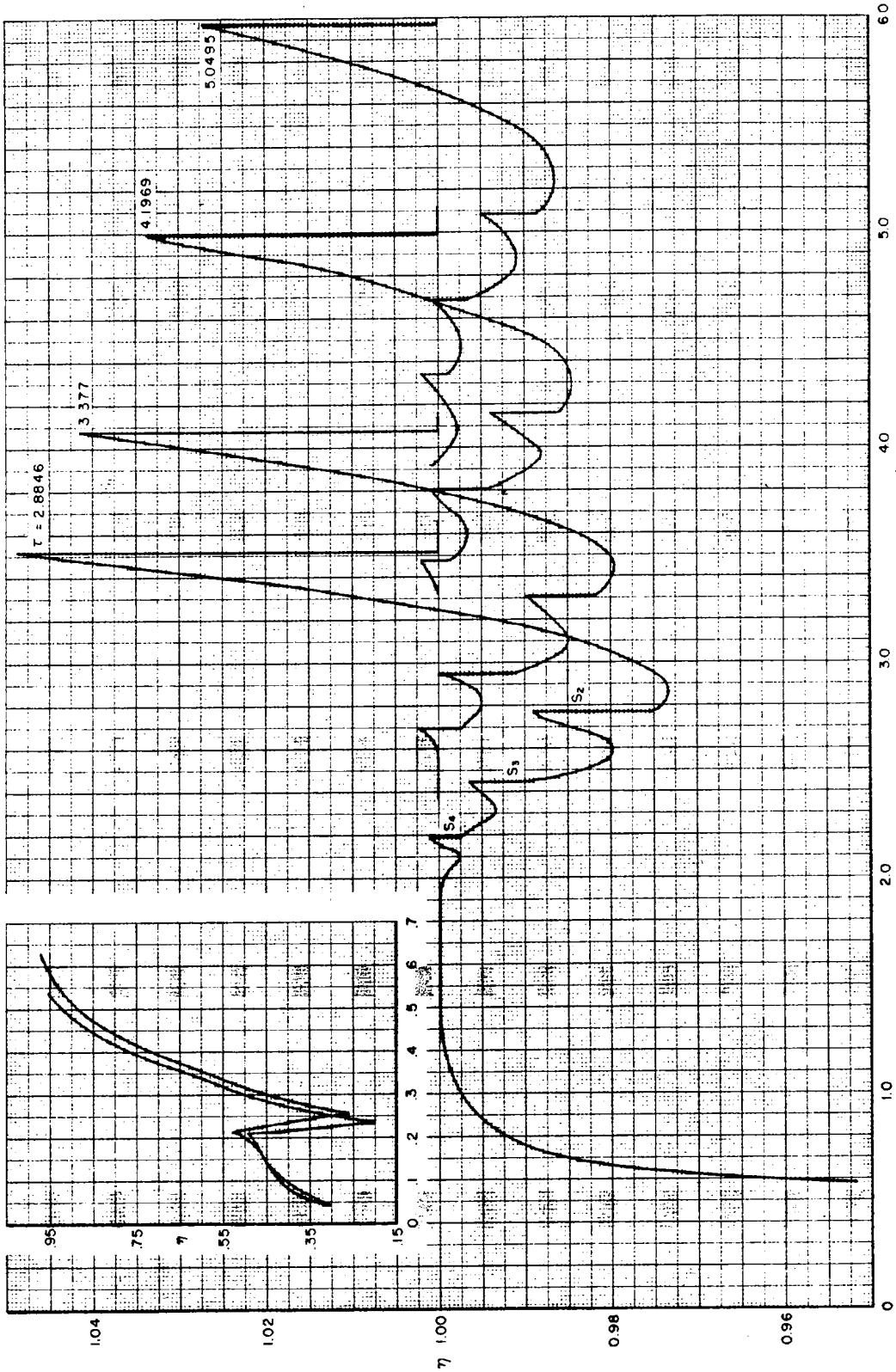

Fig. 28 — Density ($\eta = \rho/\rho_0$) vs radius ($\lambda = r/a$) at indicated times ($\tau = tc_0/a$) for a TNT blast

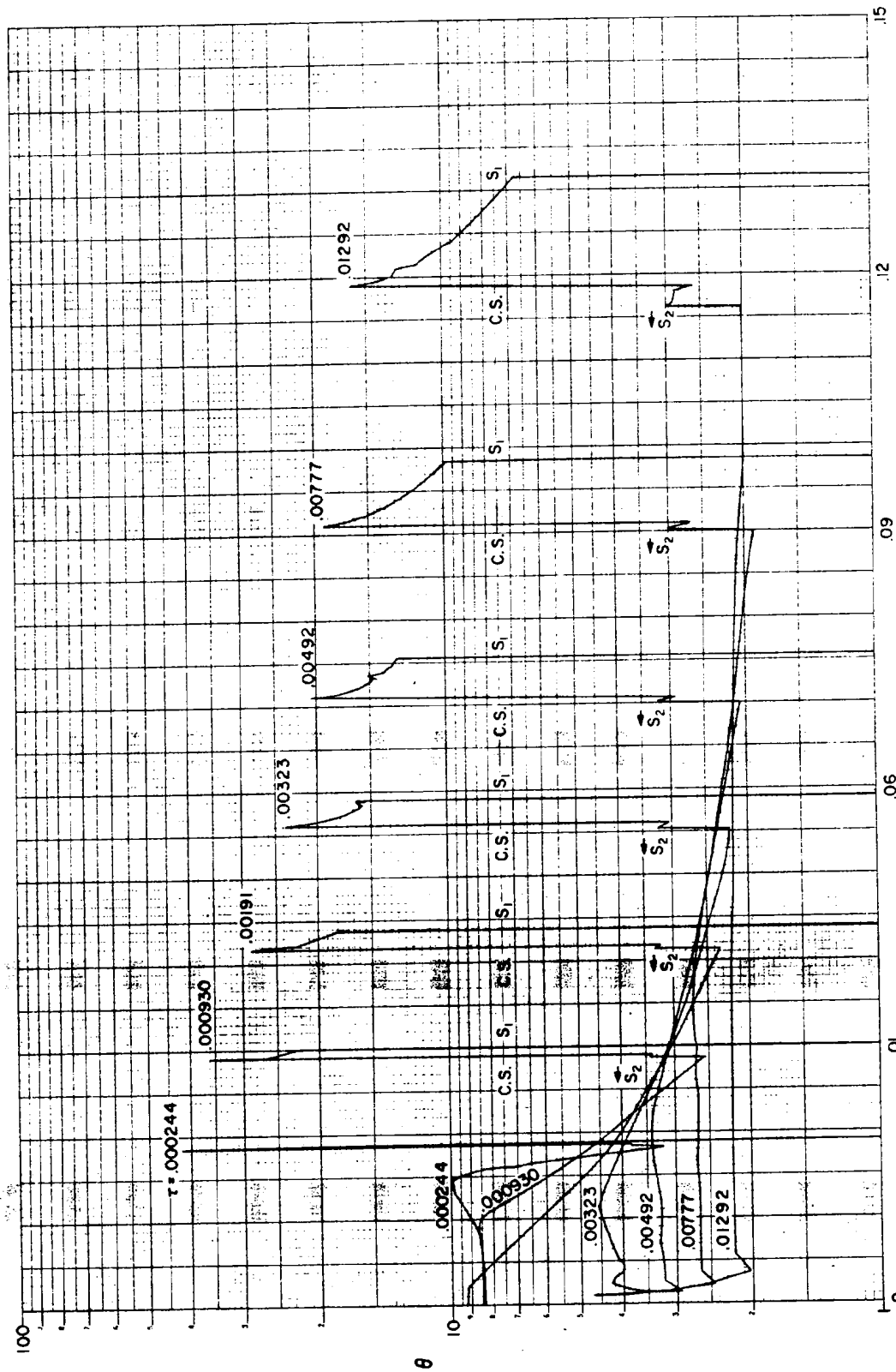

Fig. 29 — Temperature ($\theta = T/T_o$) vs radius ($\lambda = r/a$) at indicated times ($\tau = tc_o/a$) for a TNT blast ($T_o = 273.2°K$)

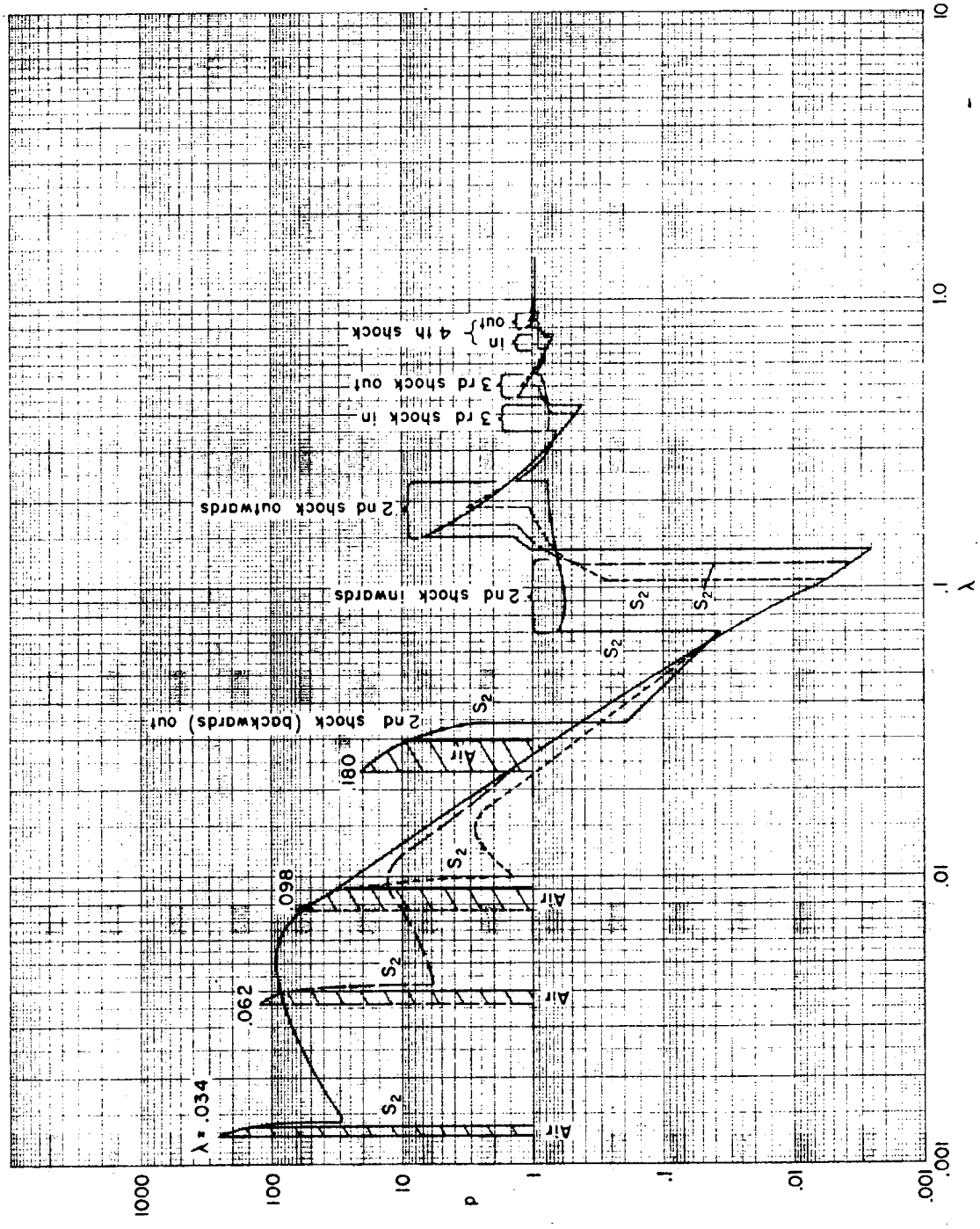

Fig. 30—Pressure vs time at indicated radii for points inside the maximum radius of the TNT gases

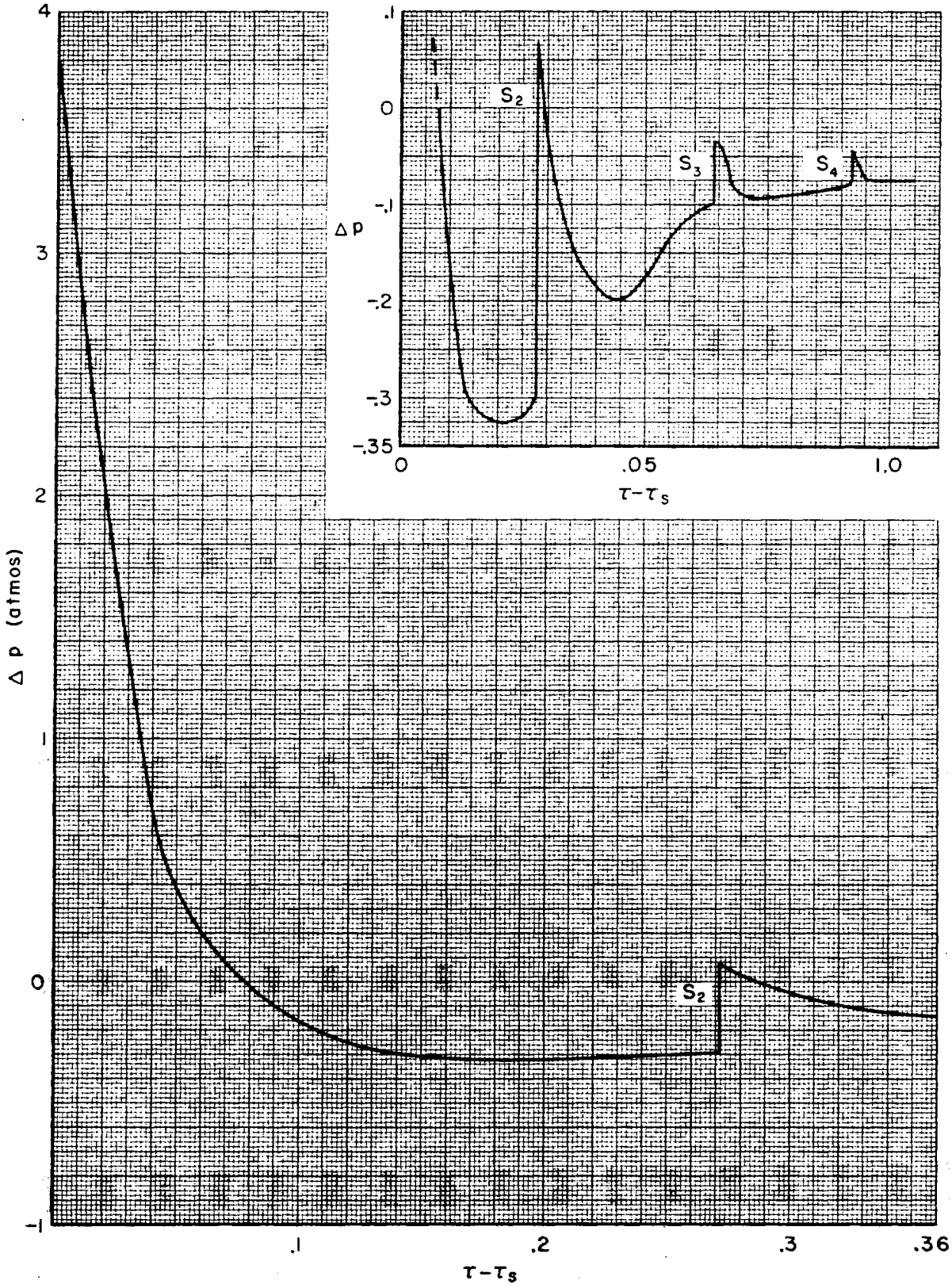

Fig.31 — Overpressure ($\Delta p = \pi - 1$) versus time aftershock arrival at radius $\lambda = 0.350$ from TNT explosion

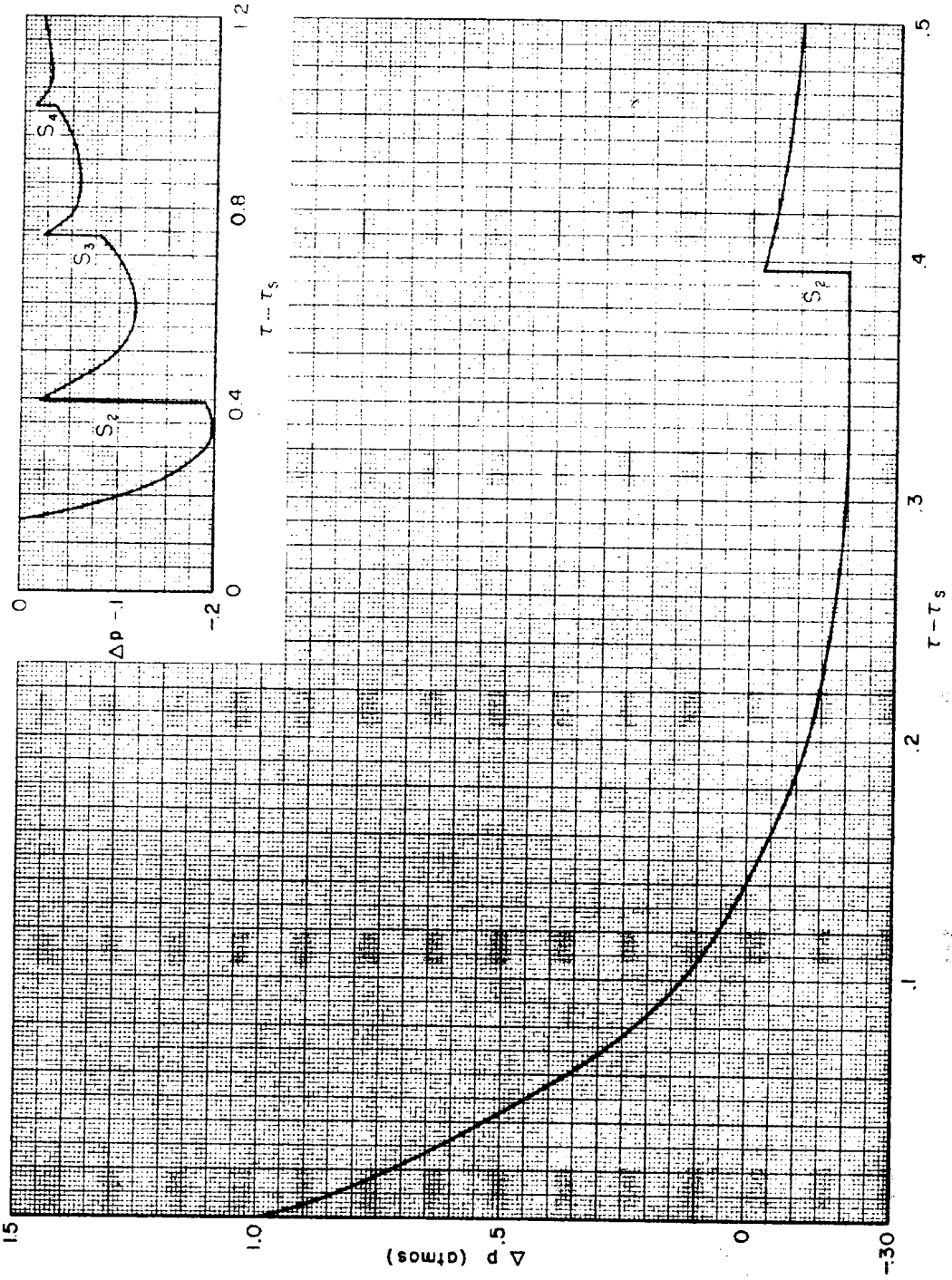

Fig.32 — Overpressure ($\Delta p = \pi - 1$) versus time aftershock arrival at radius $\lambda = 0.669$ from TNT explosion

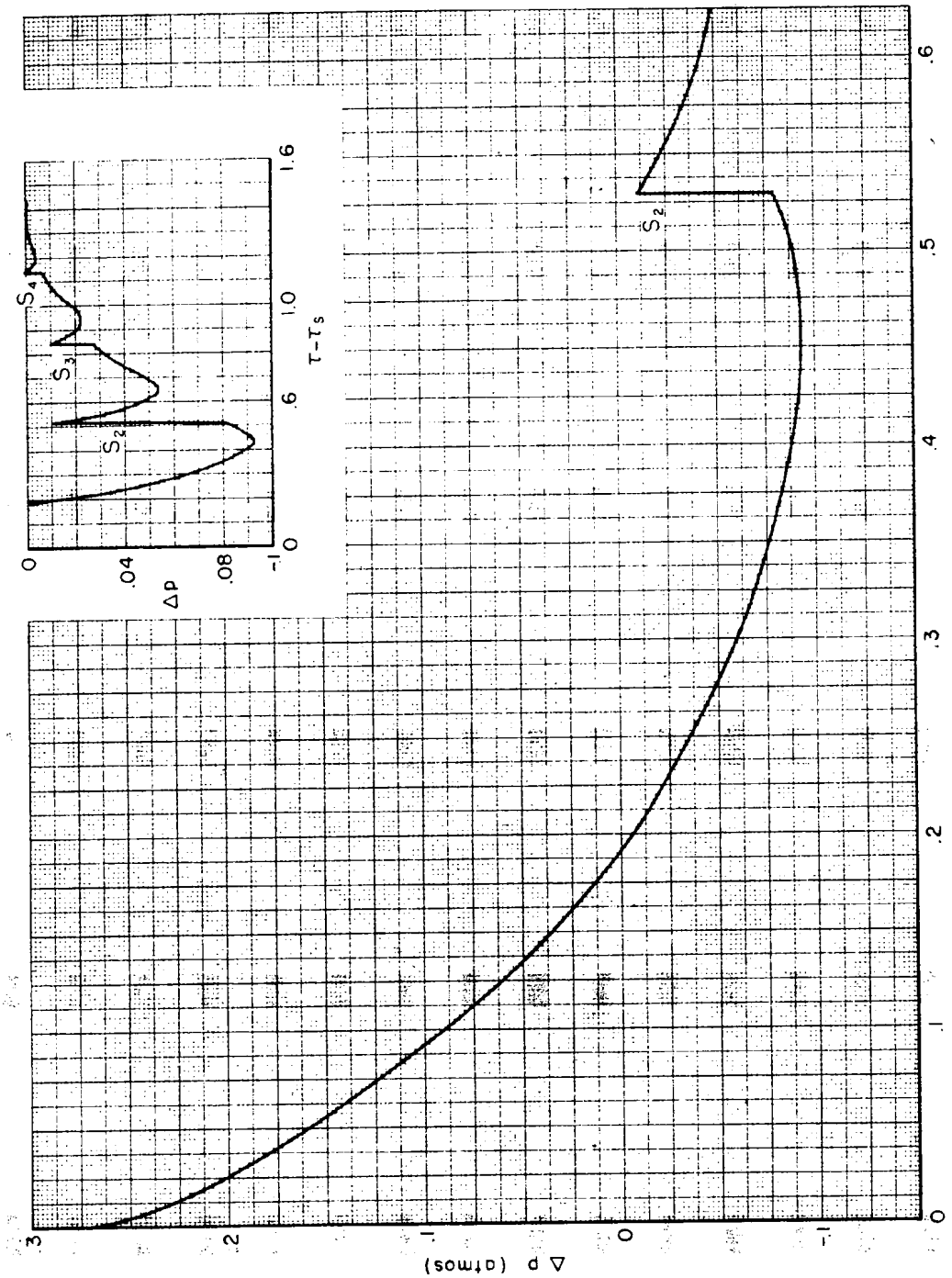

Fig.33—Overpressure ($\Delta p = \pi - 1$) versus time aftershock arrival at radius $\lambda = 1.328$ from TNT explosion

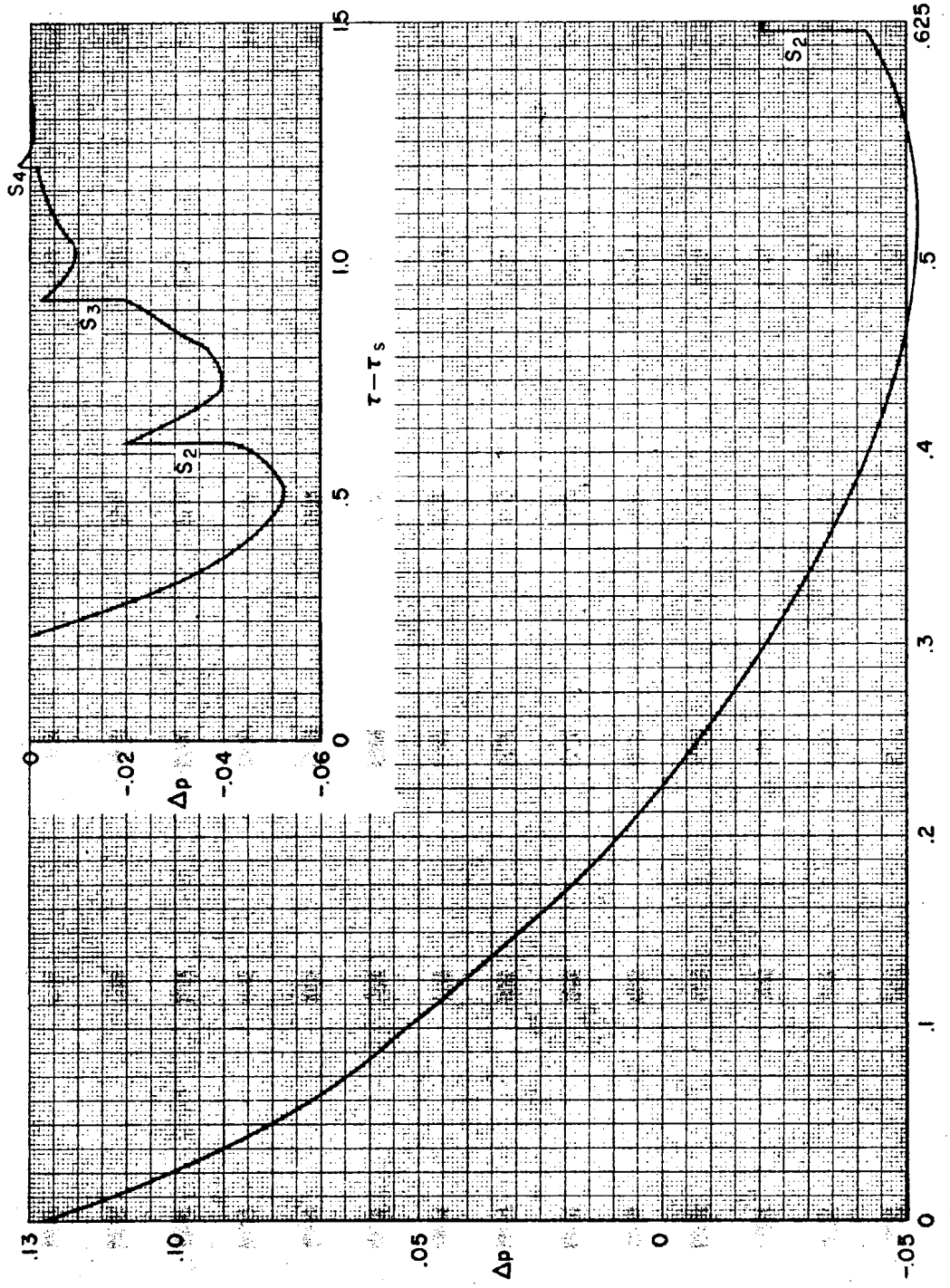

Fig. 34—Overpressure ($\Delta p = \pi = 1$) versus time after shock arrival at a radius $\lambda = 2.134$ from a TNT explosion

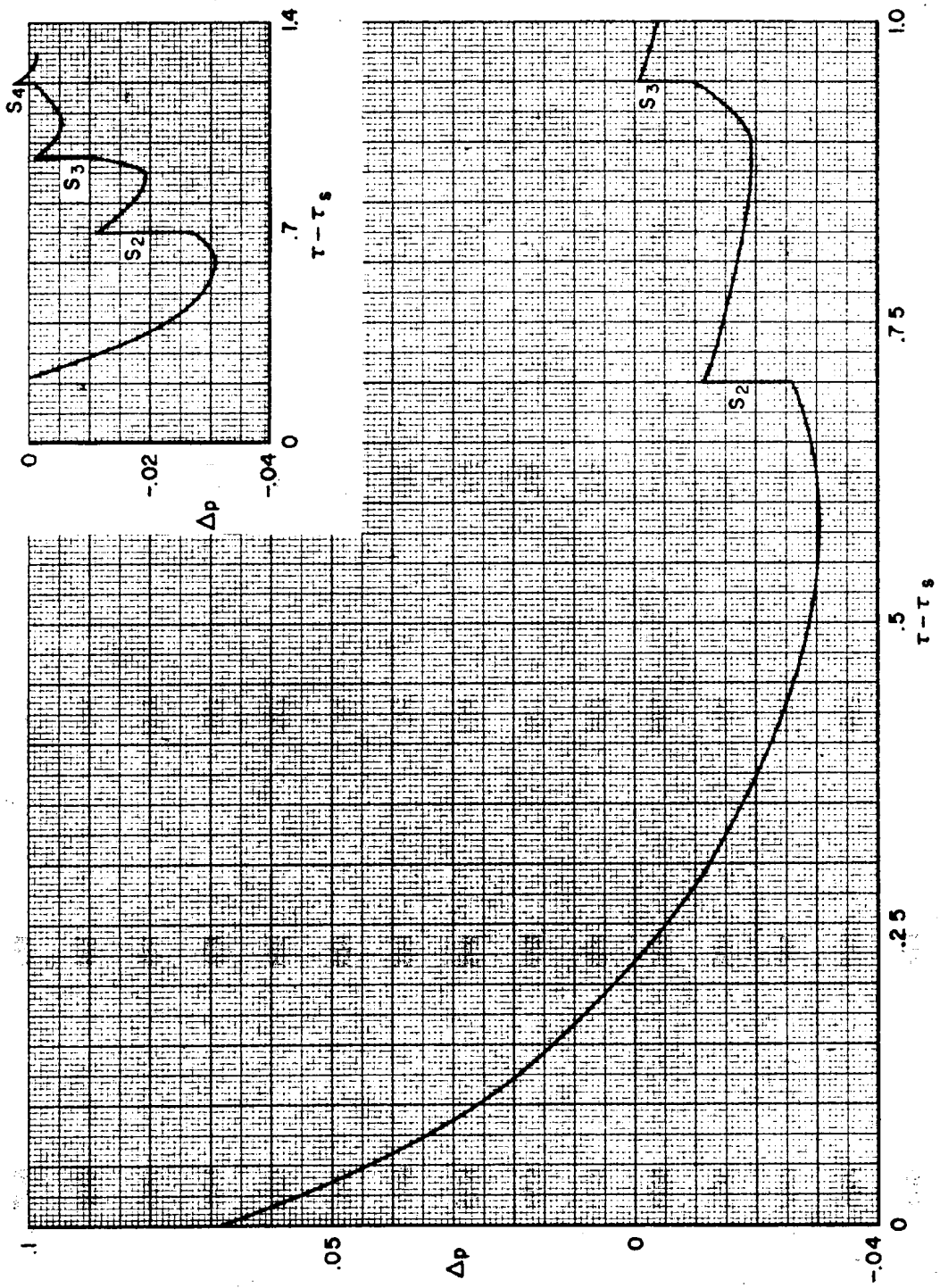

Fig. 35—Overpressure ($\Delta p = \pi = 1$) versus time after shock arrival at a radius $\lambda = 3.504$ from a TNT explosion

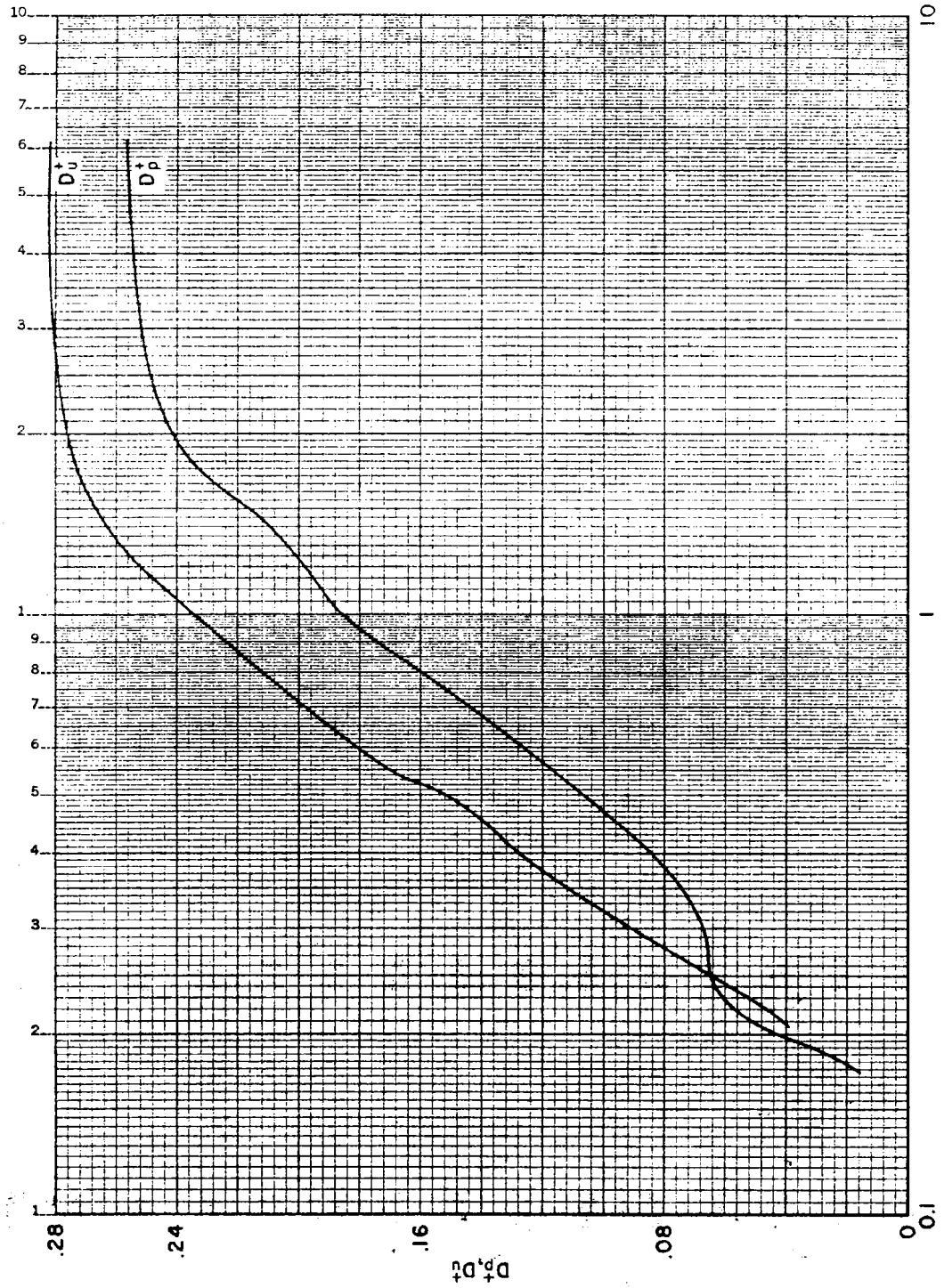

Fig. 36—Durations of positive phases of overpressure and velocity versus radius for a TNT blast

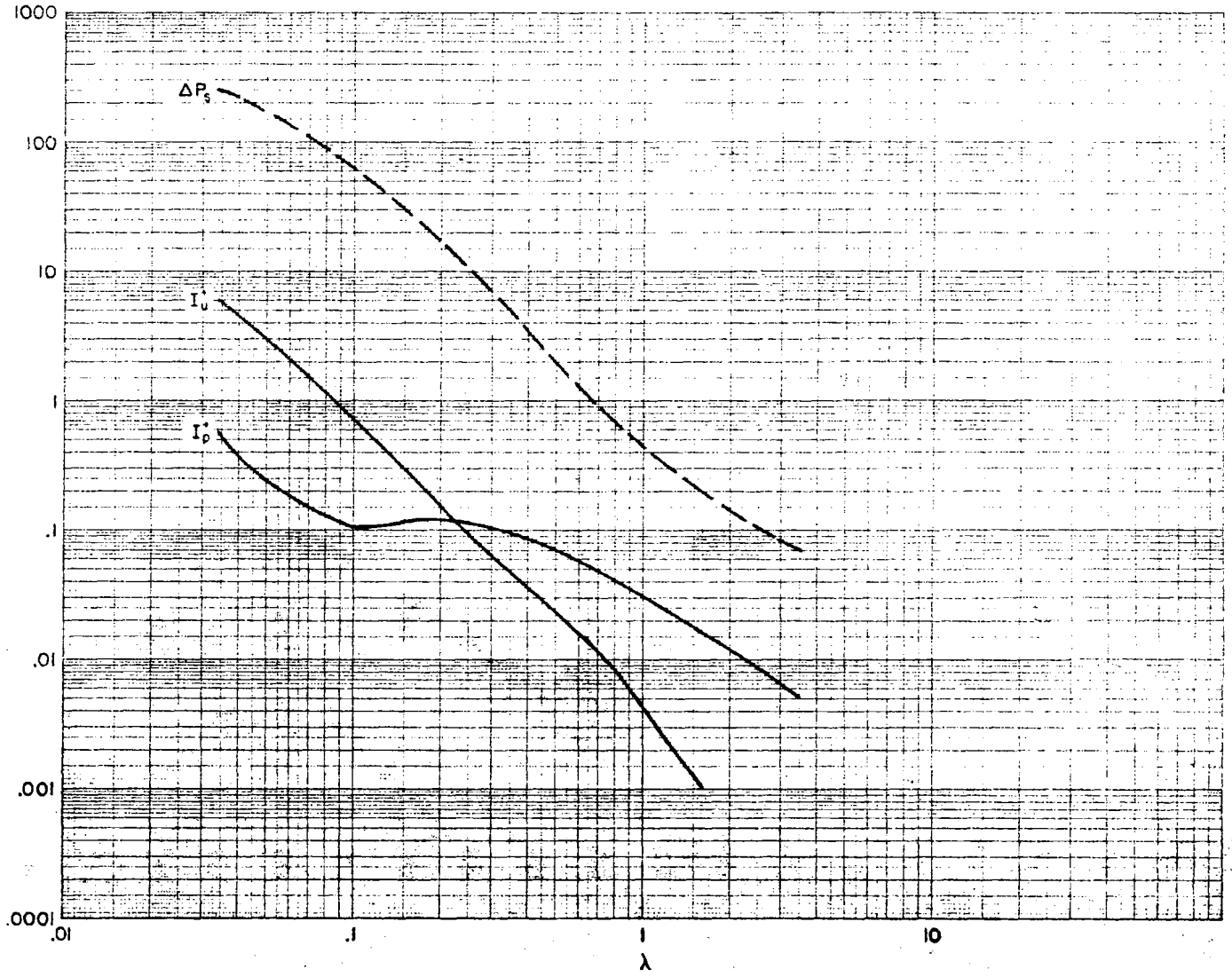

Fig. 37—Positive impulses for overpressure and dynamic pressure vs radius for a TNT blast